

# Magnetic properties and potential field modeling of the Peculiar Knob metamorphosed iron formation, South Australia: An analog for the source of the intense Martian magnetic anomalies?

Phillip W. Schmidt,<sup>1</sup> Suzanne A. McEnroe,<sup>2</sup> David A. Clark,<sup>1</sup> and Peter Robinson<sup>2</sup>

Received 9 May 2006; revised 18 August 2006; accepted 27 September 2006; published 3 March 2007.

[1] Magnetic property measurements show that the strongly metamorphosed Peculiar Knob iron formation (IF), South Australia, is coarse-grained, high-grade hematite with variable amounts of magnetite and maghemite. This body exhibits a relatively low magnetic susceptibility ( $<0.3$  SI) that cannot explain the associated intense magnetic anomaly, 30,000 nT, in terms of induced magnetization alone. Peculiar Knob IF possesses an extremely intense ( $\sim 120$  A m<sup>-1</sup>) remanence, directed steeply upward. This ancient remanence reinforces the local Earth's field (inclination  $-63^\circ$ ). A simple geological model, constrained by drilling and physical property measurements, explains both the observed magnetic and gravity anomalies, consistent with the Poisson theorem. Koenigsberger ratios (Qs) of 10 and greater, as found here, are rare in nature. We postulate that acquisition of a thermoremanent magnetization (TRM) by the ore during postmetamorphic cooling from above the Curie/Néel temperature accounts for the intense remanence and high Qs. Although the hematite is in the multidomain size range, the coercivity is higher than expected. Also, the natural remanent magnetization (NRM) values are less than 10% of the expected value for a saturated TRM of hematite. On the basis of reflected light, scanning electron microscope observations, and rock magnetism, we propose that the common fine intergrowths of a very small amount of magnetite and/or maghemite within the hematite host are responsible for the relatively high coercivity and contribute to the NRM. These intergrowths are not normal exsolution lamellae and were likely present at high temperature. This study suggests that coarse-grained hematite-rich bodies that carry TRM and have been subjected to high-grade ( $>680^\circ\text{C}$ ) metamorphism may be possible sources for some of the prominent Martian anomalies.

**Citation:** Schmidt, P. W., S. A. McEnroe, D. A. Clark, and P. Robinson (2007), Magnetic properties and potential field modeling of the Peculiar Knob metamorphosed iron formation, South Australia: An analog for the source of the intense Martian magnetic anomalies?, *J. Geophys. Res.*, *112*, B03102, doi:10.1029/2006JB004495.

## 1. Introduction

### 1.1. Background

[2] Studies of the magnetic properties of iron formations have provided much basic information on the extremes of natural magnetic behavior. Airborne magnetic surveys have been able to identify many valuable ore deposits under thick sedimentary cover because of the strong magnetic anomalies associated with iron formations. The Peculiar Knob iron formation (IF) occurs under cover within the Paleoproterozoic basement of the Mount Woods Inlier, northern Gawler craton, 85 km southeast of Coober Pedy, South Australia (Figure 1). It was discovered by airborne magnetic surveying and a follow-up ground gravity survey, both of which showed extreme anomalies. The magnetic anomaly is 30,000 nT above background. The peak total

magnetic intensity is  $\sim 90,000$  nT while the gravity anomaly is  $>50$  gravity units (GU) ( $>5$  mGal). Following diamond drilling and susceptibility logging of the drill core, magnetic modeling carried out by the exploration company (CRAE) was unable to explain the magnetic anomaly satisfactorily. The body is composed of almost pure hematite with volumetrically minor amounts of magnetite and/or maghemite. While the density contrast explained the gravity anomaly satisfactorily, the magnetic susceptibility was orders of magnitude too low to account for the anomaly, assuming that only induced magnetization caused the anomaly.

[3] A total magnetic intensity (TMI) image for the Peculiar Knob prospect is shown in Figure 2. The coincidence of the Peculiar Knob IF magnetic and gravity anomalies is of great interest from a mineral exploration point of view. Many of the magnetic target rocks of the Mt Woods Inlier are associated with base metal mineralization and Cu-Au ( $\pm$ U and Ag). The giant Olympic Dam hydrothermal Cu-U-Au-Ag ore deposit, which occurs in an enormous volume of semimassive hematite and hematite

<sup>1</sup>CSIRO Industrial Physics, Lindfield, New South Wales, Australia.

<sup>2</sup>Geological Survey of Norway, Trondheim, Norway.

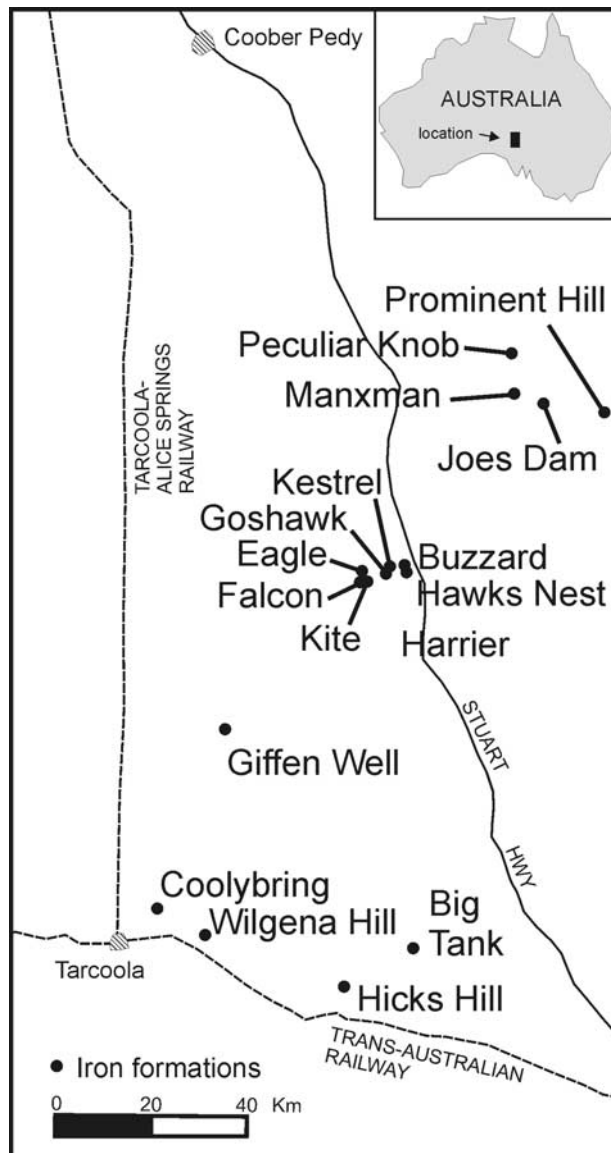


**Figure 1.** Locality map of the Peculiar Knob iron formation and other iron formations of the northern Gawler Craton.

breccia within brecciated Mesoproterozoic granite 200 km to the southeast of the Mount Woods Inlier, was identified by a coincident magnetic and gravity anomaly [Esdale *et al.*, 2003]. The large 170 GU (17 mGal) gravity high arises from the hematite-rich ore body. The nearly coincident, but broader, 1000 nT magnetic anomaly was originally interpreted as arising from a deeper body, such as a mafic intrusion, but appears to be explicable by induced magnetization of magnetite, which becomes more abundant in peripheral and deep portions of the system, possibly supplemented by remanence carried by hematite in the breccia and the extensive surrounding hematitic alteration halo.

[4] Olympic Dam-type mineralization in the region is associated with hydrothermal fluids, predominantly of magmatic origin, generated during emplacement of Mesoproterozoic (circa 1590 Ma) granites of the Hiltaba Suite. The recently discovered Prominent Hill system [Hart and

Freeman, 2003], 25 km SE of Peculiar Knob, contains a Cu-Au (U, rare earth elements (REE)) mineralized hematite breccia (Olympic Dam analog) developed within Paleoproterozoic metasedimentary rocks and felsic volcanics. A prominent gravity high is associated with the mineralized hematite-rich zone, which has a subdued magnetic response. A strong magnetic high occurs over an adjacent magnetite-rich alteration zone, separated from the hematite zone by a fault, with very little magnetic response from the hematite-rich mineralized zone.

[5] The metamorphosed IF at Peculiar Knob is under cover of 10–30 m of Cretaceous sediments and, as a result of diamond drilling, several bodies consisting of magnetite rich layers and hematite-rich layers, 15–36 m thick, dipping steeply northwest, have been identified. The Peculiar Knob IF has potential as a source of pure iron ore for grade control, i.e., to maintain specified percentages during mining.

[6] On the basis of present understanding [Morris and Hough, 1997] it appears that the Peculiar Knob IF was originally deposited as part of a banded iron formation. Later it was partially altered to massive oxide by supergene enrichment and/or hydrothermal processes. These events were followed by regional granulite-facies metamorphism and high-grade contact metamorphism, associated with emplacement of the Mesoproterozoic (circa 1590 Ma) Balta Granite. There is also the possibility of later low-grade hydrothermal alteration. The massive hematite ore at Peculiar Knob therefore has a different genesis than hydrothermal Olympic Dam-type ore bodies. The hydrothermal massive coarse-grained hematite ore at Prominent Hill has not been metamorphosed and is very weakly magnetized. Similarly, the hematite-rich hydrothermal ores of Olympic Dam do not have a strong remanent magnetization.

[7] The ground level magnetic anomaly at Peculiar Knob is in excess of 30,000 nT above background. Thus the anomaly intensity is over half the intensity of the local Earth's field. Measured susceptibilities are typically several orders of magnitude too low to account for such an intense anomaly. Downhole logging showed 50% of the body has susceptibility of 0.1 SI, or less. Magnetic properties of drill core samples were examined to test whether the anomaly could be explained by remanent magnetization, or whether the drill holes have failed to intersect the causative body. This work is based on samples from four drill cores originally studied by Schmidt [1986] that contain massive hematite/magnetite (mHt/Mt), hematitic quartzite, hematite- and magnetite-bearing granite, and amphibole gneiss layers (Table 1).

## 1.2. Consideration of Large Remanent Magnetic Anomalies on Earth in Relation to Anomalies on Mars

[8] Detailed magnetic studies of rocks that produce large magnetic anomalies on Earth are rare. In many instances the inducing vector is the dominant magnetic response, or the remanent and the inducing vector are in similar directions, and the anomaly is typically modeled using an assumed susceptibility and Koenigsberger ratio ( $Q$ ). Natural remanent magnetization (NRM) intensity is therefore implicit, but directions are not used. In the other extreme case, when the NRM vector dominates the magnetic response but is oblique to the induction, or the induced component is very low (i.e., very little magnetite), important anomalies can be

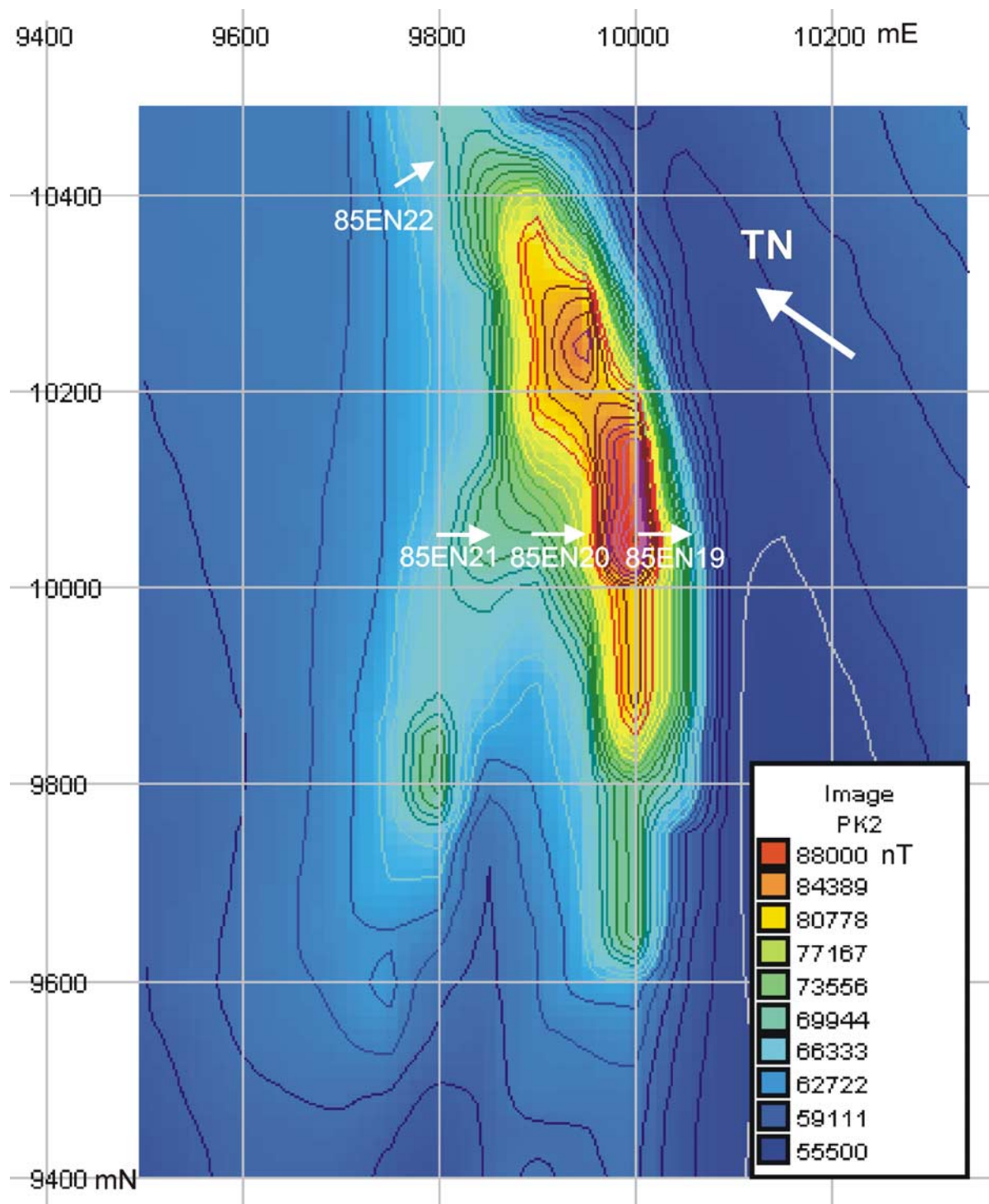


**Figure 2.** Total magnetic intensity (TMI) image of the Peculiar Knob prospect, Mount Woods Inlier, northern Gawler Craton, South Australia. Grid north is N55°E, and the magnetic units are nT. Original magnetic contours provided by CRA Exploration (now part of Rio Tinto) and digitized in house. The arrows indicate direction of drilling (i.e., nonvertical holes). Peculiar Knob is of interest in itself as a source of high-purity iron ore for grade control.

overlooked based on false assumptions. Interest in rock types that can create large remanent anomalies has now grown outside the field of exploration geophysics to encompass the larger geological community due to fascination with the discovery of large remanent magnetic anomalies on

Mars [Acuña *et al.*, 1999; Connerney *et al.*, 2004]. With few studies of the rocks and oxide minerals that create large remanent magnetic anomalies on Earth [Alva-Valdivia and Urrutia-Fucugauchi, 1995; Balsley and Buddington, 1958; Bath, 1962; Clark, 1997, 1999; Hargraves, 1959; Kelso *et*

**Table 1.** Summary of Magnetic Properties of Peculiar Knob Iron Formation<sup>a</sup>

DDH	Depth, m	Lithology	N	Inc, deg	$J$ , A m <sup>-1</sup>	$k$ , SI	Q	A
85EN19	71.3–71.4	mHt <sup>b</sup>	4	–47	204	0.0035	1230	1.44
85EN20	37.8–37.9	hematite-magnetite quartzite	3	–29	0.256	0.0292	0.18	1.09
	89.1–89.3	magnetite-hematite granite gneiss	4	6	5.09	0.2488	0.45	1.10
	90.8	amphibole gneiss	2	16	8.71	0.0131	1.4	1.18
	97.0–97.4	mHt/Mt <sup>c</sup>	6	–15	56.9	0.3368	3.71	1.27
	241.6–242.3	mHt/Mt <sup>c</sup>	9	–71	202	0.3142	14.1	1.12
	246.6–247.0	mHt/Mt <sup>c</sup>	8	–69	227	0.4034	12.3	1.04
85EN21	56.5	magnetite granite	3	–43	1.13	0.1043	0.24	1.12
	71.8–71.9	hematite-magnetite granite	3	–75	58.4	0.7025	1.82	1.17
	111.7–111.8	mHt/Mt <sup>c</sup>	4	–70	114	0.0378	66.1	1.20
85EN22	118.2–118.6	magnetic quartzite	11	–89	36.8	0.2413	3.34	1.48
	137.7	mHt/Mt <sup>c</sup>	2	–13	36.0	0.2350	3.40	1.20

<sup>a</sup>N, number of samples; Inc, inclination;  $J$ , intensity of magnetization;  $k$ , low-field magnetic susceptibility; Q, Koenigsberger ratio; A, anisotropy of magnetic susceptibility ( $k_{\max}/k_{\min}$ ).

<sup>b</sup>Massive hematite.

<sup>c</sup>Massive hematite/magnetite.

al., 1993; McEnroe and Brown, 2000; McEnroe et al., 2001a, 2001b, 2002, 2004a, 2004b, 2004c], speculation has dominated thinking about the magnetism of extraterrestrial planetary bodies. Numerous studies exist on minerals that are postulated to be responsible for the large Martian anomalies; however, most of these are based on magnetic saturation behavior [Kletetschka et al., 2000a], a high-field attribute, not a weak-field attribute, as would be expected from a planetary body in our solar system. On Earth, magnetic anomalies are created in a weak field of only  $\sim 50,000$  nT. Though arguments have been put forward for various field strengths for the primary Martian field and later residual crustal fields, all hypothesized fields are weak fields, as compared to the saturating fields of most minerals. The Martian crust is on average an order of magnitude more strongly magnetized than the Earth's crust. Magnetizations averaging typically  $\sim 20$  A m<sup>-1</sup> over huge volumes are required to explain the observed anomalies [Connerney et al., 2004]. Although very little is known about the magnetic mineralogy of the Martian crust, analyses of Martian soils and meteorites indicate that the crust is significantly more iron-rich ( $\sim 20$  wt % FeO) than average terrestrial crust. Thus, on average, Martian rocks can be expected to contain significantly higher concentrations of magnetic iron-bearing minerals than typical crustal rocks on Earth.

[9] Hargraves et al. [2001] and Kletetschka et al. [2000a] discussed which magnetic minerals could carry the intense remanent magnetization required to produce the magnetic anomalies on Mars. These might include single domain (SD) magnetite or titanomagnetite, SD pyrrhotite, and multidomain (MD) hematite. Finely exsolved members of the hematite-ilmenite series are also candidates [McEnroe and Brown, 2000; McEnroe et al., 2001a, 2001b, 2002, 2004c; Robinson et al., 2002, 2004] and finely exsolved oxides in silicates are discussed by McEnroe et al. [2004a, 2004b] and Frandsen et al. [2004]. Scott and Fuller [2004] proposed SD magnetite produced during metamorphism of iron-rich carbonates as a source of Martian magnetic anomalies.

[10] In recent years there has been a resurgence of interest in MD hematite as a carrier of intense remanence. Kletetschka et al. [2000a, 2000b] and Özdemir and Dunlop [2002, 2005] have suggested that in the Earth's field TRM of MD hematite is expected to be a substantial fraction of the saturation remanence, producing a very large NRM and

this effect would increase with grain size. However, the above studies do not report NRM values, a central issue to magnetic anomaly studies, on Earth and Mars. A full examination of a thermoremanent magnetization (TRM) origin for the Peculiar Knob IF remanence is beyond the scope of this paper and will be presented elsewhere.

[11] With the acquisition of magnetic data from Mars and the Moon, along with the vast amount of new magnetic data from satellites and the new SWARM mission for Earth, it is vital to combine studies of the magnetic mineralogy, microstructures, and detailed rock magnetic properties of rocks from areas of documented and carefully modeled magnetic anomalies. The Peculiar Knob deposit yielded an opportunity to investigate thoroughly a large remanent magnetic anomaly, combining exploration geophysical data from aeromagnetic, ground magnetic and gravity surveys, borehole measurements, paleomagnetism, and rock magnetism.

[12] In the following, we first discuss our measurements of the magnetic properties of the Peculiar Knob IF, including low-field susceptibility, magnetic remanence and its demagnetization, both high- and low-field thermomagnetic behavior and hysteresis, which thoroughly characterize the iron formation. This information is augmented by microprobe analyses which are discussed in terms of the rock magnetic properties. We then interpret this information to explain the intense magnetic anomalies associated with the Peculiar Knob IF and compare the magnetic properties with those of other documented iron formations from Australia and North America. Finally we conclude that rocks with similar properties may also explain the intense Martian anomalies.

## 2. Samples

[13] Drill core from four diamond drill holes (DDHs) were sampled. While the core was not azimuthally oriented, the hole azimuth and plunge were recorded. The diamond drill holes were 85EN19, 85EN20, 85EN21 and 85EN22. The rock types sampled included massive hematite/magnetite, hematitic quartzite, hematite- and magnetite-bearing granite and layered amphibole gneiss (Table 1). Each drill core had a large variation in the amount of oxide and in the proportions of magnetite and hematite in each interval. Massive oxide layers contain more than 90% oxide. In other rocks oxides represent a minor constituent (Table 2).

**Table 2.** Representative EMP Analyses, Cation Formulae, and Calculated End-Members of Hematite From Peculiar Knob, 246, 242-2a, and 111-7b<sup>a</sup>

Sample	Analysis											
	F	J	O	AV	F	I	AA	AO	141	151	154	184
	Weight Percent Oxide											
SiO <sub>2</sub>	0.018	0.038	0.025	0.026	0.050	0.042	0.086	0.032	0.020	0	0.022	0
TiO <sub>2</sub>	0.050	0.115	0.063	0	0.090	0.092	0.088	0.095	0.041	0.064	0.055	0.001
Al <sub>2</sub> O <sub>3</sub>	0.004	0.026	0.035	0.043	0.010	0	0.034	0	0.041	0.038	0.034	0
Cr <sub>2</sub> O <sub>3</sub>	0.004	0	0	0.054	0.040	0	0	0.032	0	0.054	0.009	0
V <sub>2</sub> O <sub>3</sub>	0	0.078	0	0.023	0	0.034	0.024	0.015	0	0.035	0.035	0.045
Fe <sub>2</sub> O <sub>3</sub>	99.955	100.211	99.473	99.812	99.600	99.504	100.164	100.904	99.704	99.902	99.707	99.911
MgO	0	0	0.019	0	0	0.007	0.017	0.006	00	0.015	0	0
NiO	0	0	0	0.014	0.030	0	0	0.019	0	0.020	0	0
Fe total	89.982	90.181	89.432	89.819	89.670	89.604	90.248	90.849	89.776	89.905	89.757	89.896
FeO	0.042	0.010	-0.075	0.007	0.048	0.069	0.119	0.054	0.061	0.012	0.040	-0.005
MnO	0	0.137	0.054	0	0.050	0.011	0.032	0	0	0	0	0
ZnO	0.028	0	0.064	0.012	0	0.021	0	0.037	0	0.007	0	0.007
CaO	0	0	0.013	0	0.010	0.017	0	0.006	0	0.016	0.007	0
Total	90.086	90.575	89.705	89.991	89.950	89.828	90.529	91.091	89.878	90.139	89.934	89.949
Total with Fe <sub>2</sub> O <sub>3</sub>	100.100	100.615	99.671	99.991	99.929	99.797	100.564	101.200	99.867	100.148	99.924	99.959
Cations/2												
Si	0.0005	0.0010	0.0007	0.0007	0.0013	0.0011	0.0023	0.0008	0.0005	0.0000	0.0006	0.0000
Ti	0.0010	0.0023	0.0013	0.0000	0.0018	0.0018	0.0018	0.0019	0.0008	0.0013	0.0011	0.0000
Al	0.0001	0.0008	0.0011	0.0014	0.0003	0.0000	0.0011	0.0000	0.0013	0.0012	0.0011	0.0000
Cr	0.0001	0.0000	0.0000	0.0011	0.0008	0.0000	0.0000	0.0007	0.0000	0.0011	0.0002	0.0000
V	0.0000	0.0017	0.0000	0.0005	0.0000	0.0007	0.0005	0.0003	0.0000	0.0007	0.0008	0.0010
Fe <sup>3+</sup>	1.9968	1.9910	1.9950	1.9957	1.9926	1.9934	1.9904	1.9936	1.9960	1.9944	1.9946	1.9990
Mg	0.0000	0.0000	0.0008	0.0000	0.0000	0.0003	0.0007	0.0002	0.0000	0.0000	0.0006	0.0000
Ni	0.0000	0.0000	0.0000	0.0003	0.0006	0.0000	0.0000	0.0004	0.0000	0.0004	0.0000	0.0000
Fe Total	1.9978	1.9912	1.9934	1.9958	1.9937	1.9949	1.9930	1.9948	1.9974	1.9946	1.9955	1.9989
Fe <sup>2+</sup>	0.0009	0.0002	-0.0017	0.0002	0.0011	0.0015	0.0026	0.0012	0.0014	0.0003	0.0009	-0.0001
Mn	0.0000	0.0031	0.0012	0.0000	0.0011	0.0003	0.0007	0.0000	0.0000	0.0000	0.0000	0.0000
Zn	0.0006	0.0000	0.0013	0.0002	0.0000	0.0004	0.0000	0.0007	0.0000	0.0001	0.0000	0.0001
Ca	0.0000	0.0000	0.0004	0.0000	0.0003	0.0005	0.0000	0.0002	0.0000	0.0005	0.0002	0.0000
Total cations total Fe	2.0000	2.0000	2.0000	2.0000	2.0000	2.0000	2.0000	2.0000	2.0000	2.0000	2.0000	2.0000
Total Fe <sup>3+</sup> Fe <sup>2+</sup>	2.0000	2.0000	2.0000	2.0000	2.0000	2.0000	2.0000	2.0000	2.0000	2.0000	2.0000	2.0000
Ox Sum	2.0016	2.0045	2.0025	2.0022	2.0037	2.0033	2.0048	2.0032	2.0020	2.0028	2.0027	2.0005
3-Ox Sum	0.9984	0.9955	0.9975	0.9978	0.9963	0.9967	0.9952	0.9968	0.9980	0.9972	0.9973	0.9995
Fe <sup>3+</sup>	1.9968	1.9910	1.9950	1.9957	1.9926	1.9934	1.9904	1.9936	1.9960	1.9944	1.9946	1.9990
Fe <sup>3+</sup> /Fe total	0.9995	0.9999	1.0008	0.9999	0.9995	0.9992	0.9987	0.9994	0.9993	0.9999	0.9996	1.0001
End-Members												
FeSiO <sub>3</sub>	0.0478	0.1003	0.0666	0.0691	0.1329	0.1118	0.2271	0.0840	0.0532	0	0.0585	0
MgTiO <sub>3</sub>	0	0	0.0755	0	0	0.0278	0.0699	0.0235	0	0	0.0594	0
NiTiO <sub>3</sub>	0	0	0	0.0299	0.0641	0	0	0.0401	0	0.0427	0	0
FeTiO <sub>3</sub>	0.0449	-0.0780	-0.2342	-0.0535	-0.0253	0.0418	0.0363	0.0354	0.0820	0.0258	0.0306	-0.0117
MnTiO <sub>3</sub>	0	0.3064	0.1219	0	0.1126	0.0248	0.0716	0	0	0	0	0
ZnTiO <sub>3</sub>	0.0549	0	0.1260	0.0235	0	0.0413	0	0.0717	0	0.0137	0	0.0137
CaTiO <sub>3</sub>	0	0	0.0371	0	0.0285	0.0485	0	0.0169	0	0.0455	0.0199	0
Sum	0.1476	0.3287	0.1929	0.0691	0.3129	0.2960	0.4019	0.2716	0.1352	0.1277	0.1684	0.0020
Fe <sub>2</sub> O <sub>3</sub>	99.8419	99.5483	99.7521	99.7824	99.6294	99.6677	99.5198	99.6794	99.8005	99.7191	99.7315	99.9500
Cr <sub>2</sub> O <sub>3</sub>	0.0042	0	0	0.0567	0.0420	0	0	0.0332	0	0.0566	0.0095	0
V <sub>2</sub> O <sub>3</sub>	0	0.0826	0	0.0245	0	0.0363	0.0254	0.0158	0	0.0372	0.0373	0.0480
Al <sub>2</sub> O <sub>3</sub>	0.0063	0.0405	0.0550	0.0673	0.0157	0	0.0529	0.0000	0.0643	0.0594	0.0533	0
Sum	99.8524	99.6713	99.8071	99.9309	99.6871	99.7040	99.5981	99.7284	99.8648	99.8723	99.8316	99.9980
Total	100.0000	100.0000	100.0000	100.0000	100.0000	100.0000	100.0000	100.0000	100.0000	100.0000	100.0000	100.0000

<sup>a</sup>All analyses were made with Fe total as wt % FeO. Sums of the analyses are given as total. Formulae were calculated based on 2 cations with Fe as FeO, and an oxygen sum ("Ox Sum") was made. The amount of oxygen needed to bring the total to the stoichiometric value of 3 is 3-Ox Sum. The amount of Fe<sup>3+</sup> ions is then 2x(3-Ox Sum) and the amount of Fe<sup>2+</sup> ions is Fe total - Fe<sup>3+</sup>. Wt % Fe<sub>2</sub>O<sub>3</sub> is calculated by ((Fe<sup>3+</sup>/Fe total) × Fe total) × 1.1113444, and wt % FeO by (1-(Fe<sup>3+</sup>/Fe total) × Fe total). After this, another sum of the analysis is given as "Total with Fe<sub>2</sub>O<sub>3</sub>." In several examples, Fe<sup>2+</sup> and FeO are listed as negative. This is an inevitable result of having nearly stoichiometric hematite with very slight analytical variations. Several additional analyses, even without negative Fe<sup>2+</sup> show negative amounts of the FeTiO<sub>3</sub> end-member. This means that the very small amounts of R<sup>2+</sup> ions are insufficient to compensate for the small calculated amounts of R<sup>4+</sup> ions, negative FeTiO<sub>3</sub> adds to the total Fe<sub>2</sub>O<sub>3</sub> end-member. For analyses 242-2a, AA and AO, the original analysis sums are 90.529 and 91.091. These analyses are in the groups that appear to be overlap analyses with magnetite or with magnetite-maghemite solid solution. They do not formulate well for hematite, giving higher sums. Samples with still higher original analysis sums close to true magnetite from sample EN111.7b are formulated successfully as magnetite in Table 3, but this approach is useless for intermediate compositions, where the character of a nonstoichiometric magnetite-maghemite solution is indicated by the total Fe analysis only.

Sections of the four drill cores were subsampled to measure the properties of each rock type or oxide layer.

[14] Selected samples were studied by reflected light microscopy and by scanning electron microscopy (SEM). Samples of massive hematite + magnetite (mHt/Mt) were further selected for chemical analyses on an electron microprobe. The massive hematite/magnetite samples may contain from  $\ll 1\%$  magnetite to  $\sim 60\%$  magnetite. Massive hematite ore samples, with little or no observable magnetite, that had low susceptibility and high NRMs  $>200 \text{ A m}^{-1}$ , were studied in detail to try to understand the nature of their magnetism.

[15] When examined in reflected light, mHt/Mt samples all show abundant coarse hematite grains, many  $>500 \mu\text{m}$  and some grains millimeter size. In the same thin section some hematite grains appeared to be nearly free of any exsolution or inclusions, other hematite grains contain relict needles of spinel. These needles may indicate that some of the hematite grains were magnetite and later oxidized to hematite. At the resolution of the optical microscope under oil in crossed-polarized light a faint but distinct pattern is observed in many massive hematite grains (Figure 3a). Twinning in the hematite is also common. These microscopic structures hint that the magnetic properties of these phases may not conform to those expected of normal “pure” hematite. In observations of polished cores of massive hematite, discrete areas of magnetite range from abundant ( $>5\%$ ) to rare ( $<0.2\%$ ) to absent. When discrete magnetite grains are present, they are commonly large ( $>100 \mu\text{m}$ ); however, smaller grains, though much less abundant, have been observed in numerous polished sections.

[16] Figure 3b shows electron backscatter image taken with a Leo 1450 VP scanning electron microscope. There is a fine texture in the hematite grains, shown by a very slight density contrast between the host hematite and a second phase. We could not determine the material causing the fine pattern, due to the very fine grain size  $\ll 1 \mu\text{m}$ . The hematite grains are well equilibrated and show triple junctions. These textures are consistent with the high-temperature metamorphism that has recrystallized the precursor iron ore. Minor silicates are present and in the SEM images these are black due to their lower density.

### 3. Rock Magnetism

#### 3.1. Laboratory Techniques

[17] Bulk susceptibility ( $k$ ) and its variation with temperature ( $k$ - $T$ ) were measured using a transformer bridge calibrated using paramagnetic salts [Ridley and Brown, 1980]. The bridge has a sensitivity of  $10^{-6}$  SI. Remanent magnetization was measured using a fluxgate spinner magnetometer (DIGICO) that has been interfaced to a PC for measurement control and data file management. The intensities of NRMs are too great for measurement on a cryogenic magnetometer using specimens of standard volume ( $\sim 10 \text{ cm}^3$ ), although after partial demagnetization a CTF cryogenic magnetometer was used. Anisotropy of magnetic susceptibility (AMS) was measured using a DIGICO Anisotropy Delineator, which has been interfaced to a PC for data manipulation. The operating system automatically

corrects results for the DIGICO calibration error noted by Veitch *et al.* [1983] and Hrouda *et al.* [1983].

[18] Thermomagnetic curves (in applied fields) were obtained using a Munich (Petersen) Variable Field Translation Balance (VFTB). A furnace/cooling unit allows samples to be measured between  $-175^\circ\text{C}$  and  $700^\circ\text{C}$ . Small chips, up to  $\sim 350 \text{ mg}$ , cut from standard palaeomagnetic specimens, were used. Hysteresis properties, isothermal remanent magnetization (IRM) and Curie temperature were measured on the same chips. Thermomagnetic curves were measured in a magnetic induction of 0.8 T on the VFTB or on a Princeton Vibrating Sample Magnetometer (VSM) with a field of 1.2 T at the Institute of Rock Magnetism in Minnesota, USA. Density measurements on selected paleomagnetic specimens were made on a Mettler Toledo AG204 Deltarange balance.

#### 3.2. Bulk Susceptibility

[19] The range in susceptibility values for the Peculiar Knob samples is extremely large from a low of 0.003 SI for the massive hematite samples to 2.1 SI units for magnetite-rich samples. Table 1 gives the average susceptibility value for the different rock types in each of the four drill cores. These values directly reflect the magnetite content of the samples, the higher the content, the higher the susceptibility. The silicate-hosted samples are relatively rich in magnetite with susceptibility values near 0.2 SI. The layered amphibole-gneiss has the lowest susceptibility values of the silicate rocks, with an average of 0.013 SI. The drill cores through the mHt/Mt layers show a distribution with the magnetite-rich samples having an average of 0.5 SI reflecting  $\sim 13\%$  magnetite [Clark, 1997], and the massive hematite-magnetite poor samples with much lower susceptibility of 0.01 SI containing a maximum of 0.5% fine-grained magnetite. Magnetite-rich samples can contain up to 40% magnetite, whereas the massive hematite samples contain little or no observable discrete magnetite. A susceptibility down hole log made by CRA shows  $\sim 85\%$  of the Peculiar Knob IF has a susceptibility of 0.2 SI or less reflecting a maximum magnetite content of  $\sim 5\%$  if the magnetite is  $>20 \mu\text{m}$  in size and up to 10% if the magnetite is  $<20 \mu\text{m}$  size, while about 50% is less than 0.1 SI.

#### 3.3. Natural Remanent Magnetization

[20] The massive hematite and mHt/Mt layers all have high natural remanent magnetization (NRM) values; however, there is significant variation in susceptibility (Table 1). DDH 85EN19 samples in sections 71.3 m to 71.4 m and DDH 85EN20 samples in sections 241.6 m to 247.0 m were found to possess extremely strong remanences. Samples in sections 71.3 m to 71.4 m have consistent NRM values of  $\sim 200 \text{ A m}^{-1}$  and susceptibility values of 0.0035. In section 241.6 m to 247.0 m, samples have a large range in both NRMs, from 70 to  $270 \text{ A m}^{-1}$ , and susceptibility values from 0.0080 to 2.133 SI. Samples in drill core DDH 85EN21 from 111.7 to 111.8 m have NRMs from 99 to 165 and susceptibility values from 0.0165 to 0.1222. The two remaining mHt/Mt drill core sections (DDH 85EN20, section 97.0 m to 97.4 m, and DDH 85EN22, at 137.7 m) and a magnetic quartzite at 118.2 m to 118.6 m were magnetite-rich with 6–24% magnetite,  $\sim 36$ – $57 \text{ A m}^{-1}$  remanence and 0.24–0.34 SI susceptibility. Other rock

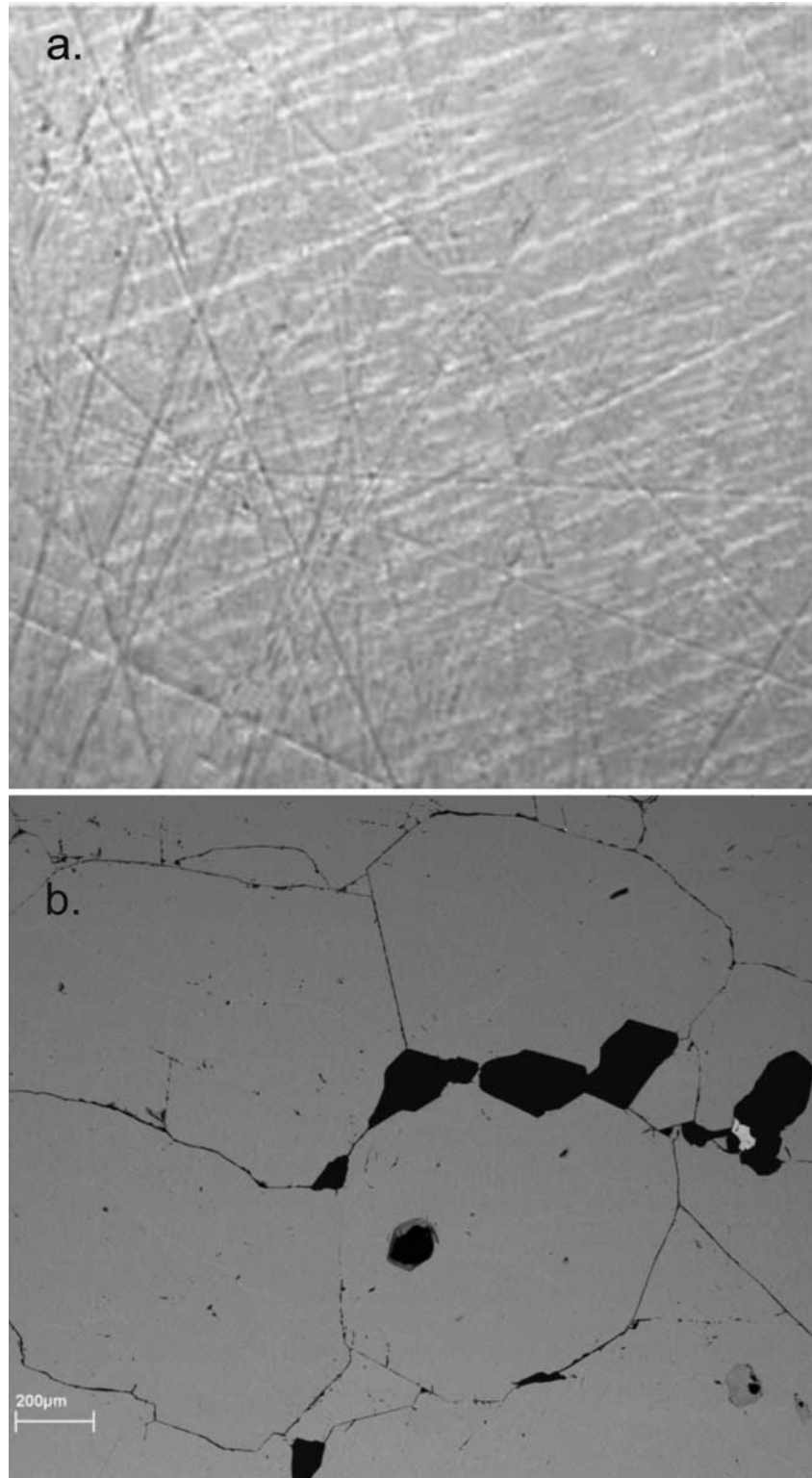


**Figure 3.** (a) Reflected light image of massive hematite sample 242.2a with a very fine microstructure. Fine-scale texture is only visible in cross-polarized light due to the contrast in anisotropy. The hematite host is oriented in the direction of lowest reflectivity so that the minor intergrown phase appears lighter. Photographed with a blue filter at 100 $\times$ . (b) Electron back scatter image showing large hematite grains with very fine microstructure indicating a slight density contrast. Black grains are silicates. Scale bar is 200  $\mu\text{m}$ .

types such as hematite-magnetite quartzite, hematite-granite-gneiss, amphibole-gneiss, and magnetic quartzite possessed more moderate properties with  $\sim 0.25\text{--}5.8\text{ A m}^{-1}$  remanence and  $0.029\text{--}0.34$  SI susceptibility and much lower Koenigsberger ratios. Remanence directions of these rock types were also more scattered (between contiguous specimens) than those of mHt/Mt samples.

### 3.4. AF Demagnetization

[21] Although the drill cores were not azimuthally oriented, the directions of remanence between contiguous samples were in agreement, suggesting that the remanence is stable. Further evidence of stability was sought from alternating field (AF) demagnetization. Figures 4a–4e show stereographic projections of magnetization directions with respect to the drill core axis for NRM and after AF cleaning in peak fields of 5, 10, 20, 50, and 100 mT. Samples of mHt/Mt with low susceptibilities ( $<0.013$  SI) change direction very little up to 100 mT and have a median destructive field (MDF) of 50 mT or greater thus demonstrating remarkable stability. The stability is further borne out by intensity decay curves plotted in Figure 4f. Two samples 20/97.0b and 20/97.2a are contrastingly softer, and decay to 10–20% of their NRM intensities by 10 mT. Samples from this section of drill core EN8520 contained  $\sim 7\%$  and  $24\%$  magnetite. Figure 4b shows that this decay is accompanied by a large change in direction indicating that these samples possess multicomponent magnetization. The softer component is entirely removed by 50 mT, isolating a hard remanent component comparable in inclination to the single component magnetizations carried by the more stable mHt/Mt samples. For samples whose directions change during AF cleaning, the inclinations consistently become steeper. Because these drill cores are not azimuthally oriented, comparisons of declination are only relevant between contiguous samples. Another mHt/Mt sample which displayed anomalously low inclinations is 22/137.7 (Figure 5a), although these did not respond to AF cleaning to yield steep inclinations like 20/97.0 and 20/97.2.

[22] Magnetization directions from granite and quartzite samples (Figures 4d–4e) tend to be less systematic and less stable than those of the mHt/Mt samples, although consistent negative inclinations suggest that, overall, the intersected units are magnetized in a normal sense. Some of these rock types are reasonably magnetic and in the absence of the massive oxide layers would produce substantial magnetic anomalies themselves, i.e., the hematite-magnetite-quartzite sample from 118.2 to 118.6 m from 85EN22 has a  $Q$  of 3.3 and carries a remanence of  $37\text{ A m}^{-1}$ , which is comparable to the magnetization of young mid-oceanic ridge basalts.

### 3.5. Summary of Bulk Magnetic Properties

[23] The magnetic properties of drill cores from the Peculiar Knob iron formation are summarized in Table 1. It is apparent that the remanence of the massive oxides dominates the magnetization in this area, with Königsberger ratios ( $Q$  values) ranging from over 3 to 1230 and  $>10$  being common. Within the mHt/Mt layers there are hematite-rich and magnetite-poor specimens with susceptibilities only about  $3 \times 10^{-3}$  SI. Other samples, containing  $\sim 12\%$  magnetite, have significant susceptibilities of

$0.4$  SI, with induced magnetizations of up to  $20\text{ A m}^{-1}$ . Although large, the induced magnetizations are an order of magnitude smaller than the remanent magnetizations of up to  $270\text{ A m}^{-1}$ .

[24] Directions of stable remanent magnetization of mHt/Mt samples are plotted in Figure 5a with respect to the drill core axes. There is a clear disposition toward high inclinations indicating that the remanence is directed close to the drill core axes. Apart from samples 20/97.0 and 20/97.2 these remanent magnetizations are far too stable to be drilling-induced remanences (DIR) that are typically aligned with drill core axes as discussed by *Pinto and McWilliams* [1990]. Furthermore, the stable components are not parallel to the drill hole axis, but lie about  $20^\circ$  from it. Soft components, if present, are highly oblique to the axis and are probably random components acquired post drilling due, for example, to logging with pencil magnets.

[25] When only inclination data are available, the method of *McFadden and Reid* [1982] may be used to estimate the mean inclination and its error. This method overcomes the bias that would result from a simple arithmetic mean. The mean and its error have been used to construct an annulus that encloses the direction of the true mean remanent magnetization present at Peculiar Knob (Figure 5b).

[26] When calculating the average intensity of magnetization for magnetic modeling purposes it is normal to use the vector mean. However, here we have no declination information, so this is not possible and we have resorted to the arithmetic mean but have rejected samples which have directions with low inclinations. If it were possible to include these in a proper vector mean, these samples, whose directions are almost perpendicular to the dominant direction, would not contribute significantly. Disregarding samples from DDH 85EN20 at depths 97.0–97.4 m and DDH 85EN22 at 137.7 m, which have anomalous inclinations, display multicomponent remanences, and have low MDFs, the mean intensity of magnetization of the remaining massive Ht/Mt samples is  $190 \pm 70\text{ A m}^{-1}$ . While the inclusion of the rejected samples in an arithmetic mean would lead to the lower estimated mean of  $140\text{ A m}^{-1}$ , this would be fortuitous and we argue that it is more correct to disregard them.

[27] It is expected that  $190 \pm 70\text{ A m}^{-1}$  will be biased on the high side compared with the true average remanent intensity of these bodies because samples were selected on the basis that they appeared to have either strong remanence and/or high susceptibility. Modeling is more consistent with an average intensity of  $120\text{ A m}^{-1}$  (see section 5).

### 3.6. Low-Temperature Demagnetization

[28] Low-temperature demagnetization (LTD) using dry-ice ( $193\text{ K} - 80\text{ C}$ ) was carried out because this temperature is below the Morin transition for hematite ( $263\text{ K} - 10\text{ C}$ ), but above the Verwey transition ( $120\text{ K} - 152\text{ C}$ ) for magnetite. Experiments were made in a field free environment and provide an indication of phases present.

[29] Massive oxide samples with low susceptibilities lose about 34–43% of their NRM at dry ice temperature. Samples were then cooled in a bath of liquid nitrogen ( $77\text{ K} - 196\text{ C}$ ) and warmed back to room temperature in field-free conditions. These samples lost nearly 50% when warmed back to room temperature. These results show that

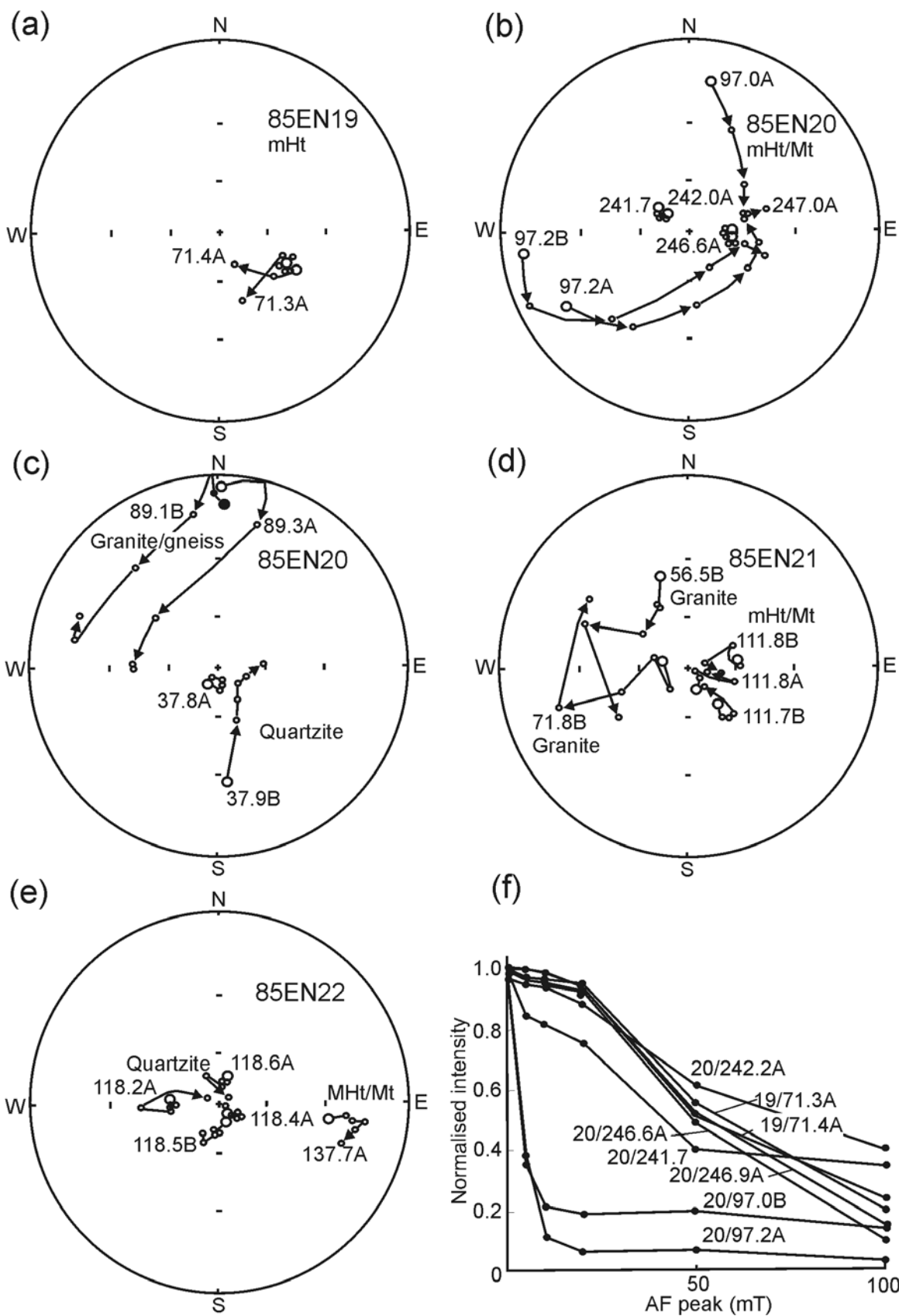


**Figure 4.** (a–e) Stereographic projections of magnetization directions for samples with respect to the drill core axis for NRM and AF demagnetization at peak fields of 2, 5, 10, 20, 50, and 100 mT. Open (solid) circles plot on the upper (lower) hemisphere. (f) Intensity demagnetization versus peak AF field strength.

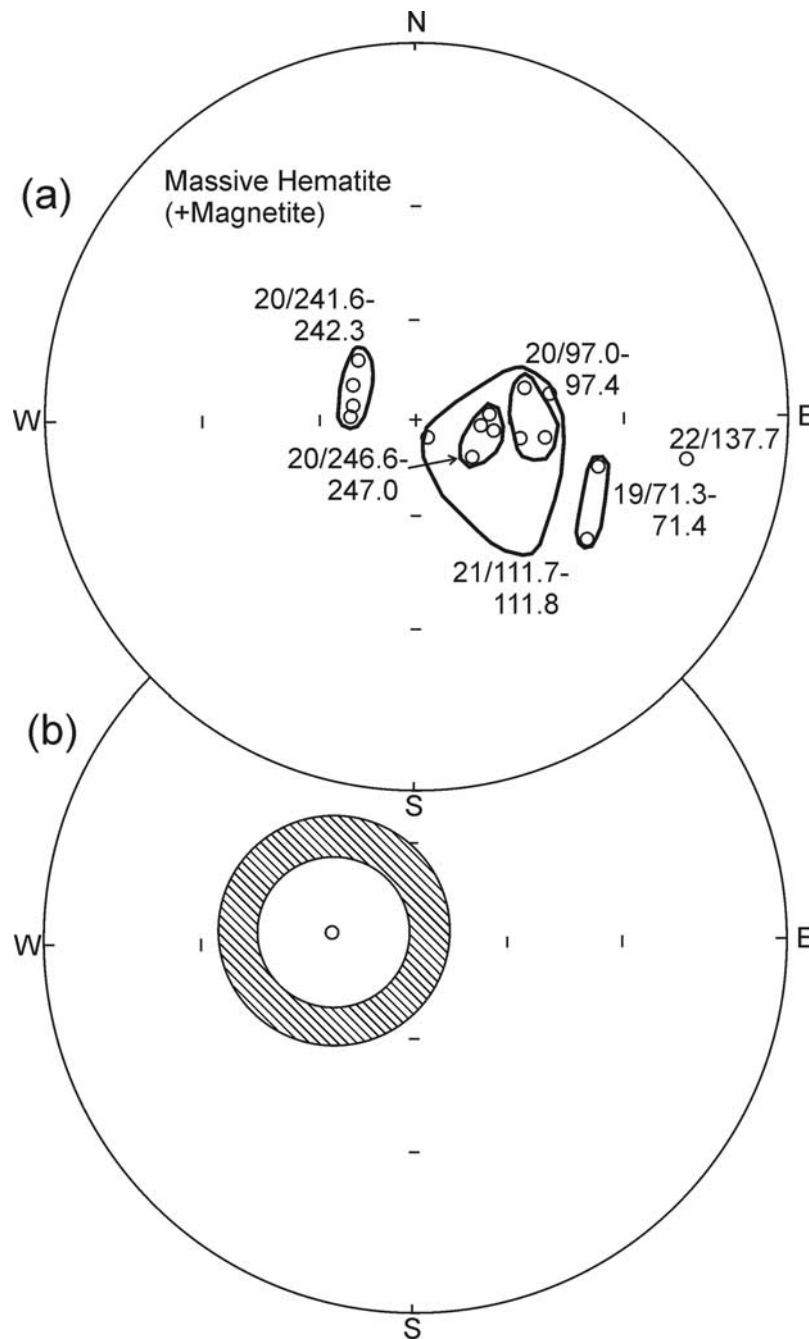


**Figure 5.** Stereographic projections of cleaned magnetization directions (symbols as for Figure 4). (a) Directions plotted with respect to drill core axis. Those in groups are from contiguous core pieces for which relative declinations could be determined. (b) Drill core axis oriented in its field position (upper hemisphere only shown). The possible magnetic remanence directions are found by constructing cones with respect to the drill core axis using the mean inclination and its error following the method of *McFadden and Reid* [1982].

the NRM of these samples is complicated and carried by more than one phase. AF demagnetization up to 90 mT followed the LTD treatment. The hematite-rich samples showed a decay up to 20 mT, followed by an increase in magnetization until 40 mT, and then a stable magnetic component to 90 mT.

[30] The hematite-magnetite-quartzite sample with 5% magnetite showed little change in magnetization with cool-

ing to  $-80^{\circ}\text{C}$  and a 90% recovery after liquid nitrogen treatment ( $-196^{\circ}\text{C}$ ). The large recovery in magnetization in both cases may indicate that the hematite is effectively coupled to a second phase, either magnetite or maghemite, which is aiding in the recovery of magnetic memory through the low-temperature cooling. A strong internal stresses due to defects, such as dislocations in the structure or mismatches in cell sizes between the hematite matrix and

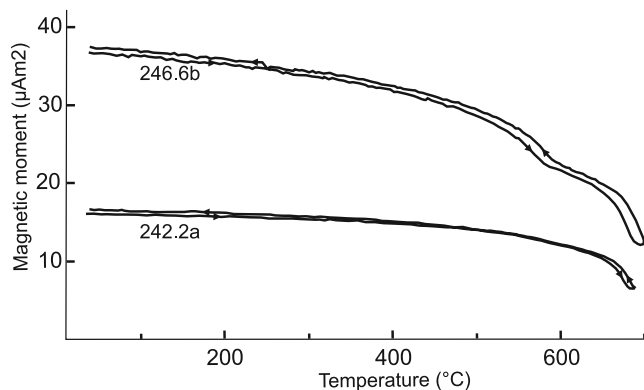


**Figure 6.** Thermomagnetic curves for massive hematite-magnetite (samples 242.2a and 246.6b) made in a 1.2 T field.

the other phase(s) could inhibit the loss of memory during low-temperature cycling.

### 3.7. Thermomagnetic Curves

[31] Saturation magnetization was measured as a function of temperature from 30°C to >690°C. Massive hematite-magnetite samples with high susceptibility show dual Curie/Néel points at 560–580°C and ~670–690°C. Samples of massive hematite with susceptibility values less than  $5 \times 10^{-3}$  SI produce a Curie-Néel point between 680–690°C. Some of these samples also show a slight decrease in intensity near 580°C, indicating the presence of magnetite. The silicate-rich samples contain hematite, magnetite or both oxides. All curves indicate that magnetite and hematite are pure phases, or close to end-member. Many of the curves, but not all, are reversible and are concave-down (Figure 6). Some samples show a slight increase in magnetization during the cooling cycle.

### 3.8. Temperature Susceptibility

[32] Figure 7a shows the k-T result from liquid nitrogen temperature (−196°C) to ~700°C on sample mHt/mt sample 247.0. The small peak observed at about −155°C is the Verwey transition indicative of the presence of MD magnetite, or equidimensional SD magnetite grains that have negligible shape anisotropy). Just below 300°C the susceptibility decreases irreversibly (as shown by alternatively cooling and reheating), reflecting chemical alteration. The most likely candidate for this alteration is the breakdown of maghemite, which is known to invert to much less magnetic hematite above 300°C. The steady irreversible increase in susceptibility above 400°C until about 500°C indicates further alteration, producing a more magnetic phase, compensating for the loss of maghemite. The more magnetic phase appears to be magnetite, as indicated by the single Curie temperature at 578°C on cooling below 600°C. On further heating another Curie point is observed at about 680°C, indicating the presence of hematite. Although the hematite signal is very much smaller than that of the magnetite, hematite is nevertheless volumetrically the dominant phase.

[33] Figure 7b shows the temperature susceptibility result from −196°C to ~700°C for a massive hematite/magnetite sample 242.2a with a bulk susceptibility of about 0.01 SI.

At low temperatures, there is no evidence for a Verwey transition, indicating that the magnetite is present in only minor amounts and likely as single domain size. Little change in magnetization occurs until ~−30°C where the susceptibility increases sharply with warming due to the Morin transition in hematite. A reversible steady increase in magnetization occurs between room temperature and ~400°C, followed by an irreversible sharp increase in susceptibility due to production of a small amount of magnetite and due in addition to a sharp Hopkinson peak for magnetite. With continued heating a sharp decrease in susceptibility indicates the Curie point of magnetite. This is then followed by a sharp increase in magnetization (a Hopkinson peak) as the Curie point of hematite is approached, followed by a rapid decay of susceptibility as the hematite loses all magnetization near 670°C. Although hematite is clearly present in unheated samples, the amount of magnetite originally present compared to that produced by heating is not clear.

[34] A thermomagnetic run on a companion chip (Figure 6, sample 242.2a) shows only a very slight decay near 580°C, with the dominant loss in magnetization near 680°C.

### 3.9. Hysteresis Properties

[35] An important consideration here, as with the J-T and J-X measurements, is the size of the sample used in the hysteresis experiments. It was small compared with the paleomagnetic specimens on which the bulk magnetic properties were measured. The bulk properties reflect the

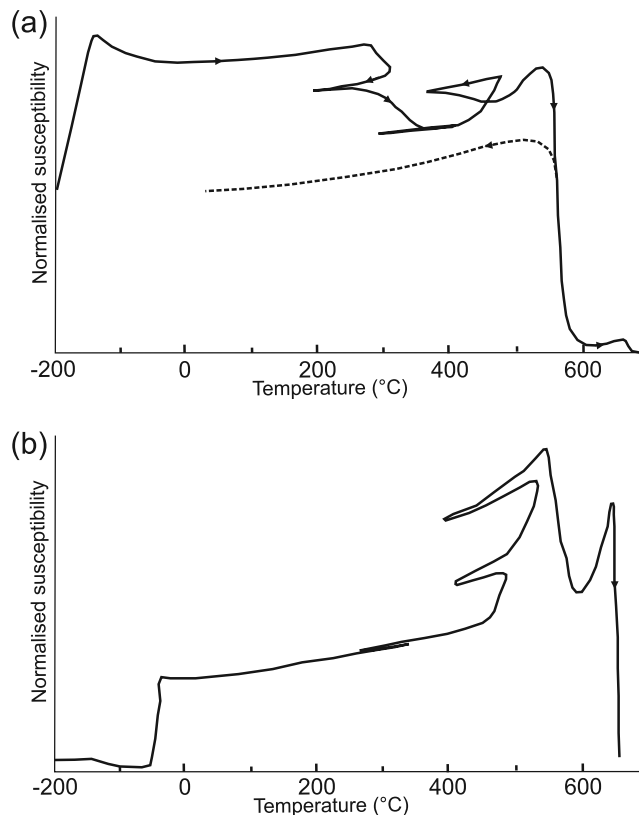


**Figure 7.** Susceptibility versus temperature (k/T) curve for massive hematite-magnetite samples (a) 247.0 and (b) 242.2a.

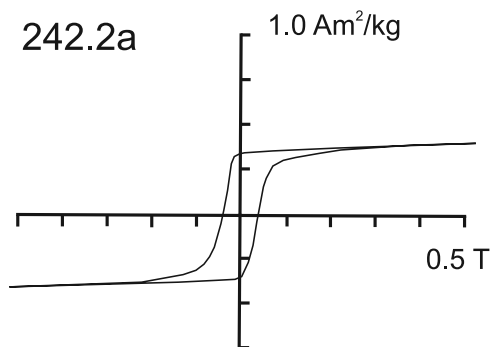


**Figure 8.** Room temperature hysteresis plot for massive hematite-magnetite sample 242.2a. The horizontal axis denotes the applied field ( $H$ ) in teslas; the vertical axis represents magnetization in  $A\ m^2\ kg^{-1}$ .

whole specimen, whereas the chips used for hysteresis measurements may not reflect the entire population in the paleomagnetic specimen. Numerous hysteresis measurements were made from different chips from the same sample to characterize the bulk sample better.

[36] Room temperature hysteresis loops for massive hematite-magnetite samples with low susceptibility values from  $3 \times 10^{-3}$  SI to  $1.2 \times 10^{-2}$  SI are similar (Figure 8). These samples have saturation magnetization ( $M_s$ ) values from  $270$  to  $326 \times 10^{-3}$   $A\ m^2/kg$  and saturation remanence ( $M_{rs}$ ) values from  $220$  to  $258 \times 10^{-3}$   $A\ m^2/kg$ . The ( $M_{rs}/M_s$ ) ratios are very high, from  $0.79$  to  $0.90$  (Figure 9). Coercive force ( $\mu_0 H_c$ ) values range from  $17$  to  $38$  mT and coercivity of remanence ( $\mu_0 H_{cr}$ ) from  $27$  to  $38$  mT. Most  $H_{cr}$  and  $H_c$  values are very similar resulting in  $H_{cr}/H_c$  ratios close to 1. The  $M_s$  values are lower than expected indicating the samples are not fully saturated in the applied field. Sample ratios are plotted in Figure 9.

[37] The massive hematite samples such as 242.2a all show rectangular shaped hysteresis loops and are clearly dominated by the antiferromagnetic hematite. The amount of magnetite is interpreted to be small because there is only a minor loss in magnetization in many of the  $J_s$  curves (high field) below  $670^\circ C$ , the bulk susceptibilities are low, and the  $k$ - $T$  curves indicate little magnetite in the samples prior to heating. However, temperature-susceptibility measurements on some samples show an increase in magnetization just below  $\sim 570^\circ C$  attributed to a Hopkinson peak for fine-grained magnetite (Figure 7). Because single-domain magnetite could have a coercivity of saturation ( $H_c$ ) near the  $H_c$  values measured here, little shape effect may be evident in the hysteresis loop.

[38] MD hematite has a rectangular shaped hysteresis loop but the bulk coercivities measured in these samples, up to  $38$  mT, are too high to reflect a multidomain structure. First-order reversal curves (FORC) show a distribution in coercivity ranging from  $10$  to  $60$  mT [McEnroe et al., 2005a, 2005b]. SEM observations of three samples from this group showed a very fine texture due to a density contrast between two phases, which we interpret to be an intergrowth of two Fe-rich phases. Such intergrowths would be expected to increase the coercivity, both by enhancing internal stresses due to lattice mismatch and by providing strong pinning sites for domain walls. If a magnetite or a

maghemite is effectively coupled to the hematite, it is possible that magnetization is retained to high temperatures and the fine microstructures are affecting the coercivity. High-temperature stability of maghemite to  $\sim 712^\circ C$  has been demonstrated recently [Brown et al., 2005].

[39] Samples with high susceptibilities ( $>0.19$  SI) contain abundant ( $>5\%$ ) magnetite.  $M_s$  values for these samples are much higher than the low-susceptibility massive hematite samples.  $M_s$  values range from  $1420$  to  $3763\ A\ m^{-1}$  and  $M_{rs}$  values from  $288$  to  $373\ A\ m^{-1}$ .  $M_{rs}/M_s$  ratios are low, from  $0.07$  to  $0.2$ . Coercivity ( $\mu_0 H_c$ ) values range from  $6$  to  $15$  mT and coercivity of remanence ( $\mu_0 H_{cr}$ ) from  $20$  to  $60$  mT.  $H_{cr}/H_c$  ratios are high, from  $1.8$  to  $8.8$ . At room temperature, hysteresis loops are symmetrical about the origin. Some samples, though dominated by magnetite, show a wasp-waisted character indicating mixed domain states.

## 4. Mineral Chemistry

### 4.1. Electron Microprobe Data

[40] Electron microprobe analyses were performed on three polished massive hematite/magnetite samples from Peculiar Knob; 246.6b and 242.2a at Macquarie University, Sydney, Australia; 111.7b at Bayerisches Geoinstitut, Universität Bayreuth, Germany. Representative analyses are shown in Tables 2 and 3. The samples were chosen because of their unusual magnetic properties, in particular the very high NRM values. All analyses indicate extremely pure Fe oxide. To demonstrate this, we cite the maximum measured value in weight% for the following oxides in the 160 accepted analyses:  $SiO_2$ ,  $0.085$ ;  $TiO_2$ ,  $0.119$ ;  $Al_2O_3$ ,  $0.085$ ;  $Cr_2O_3$ ,  $0.064$ ;  $MnO$ ,  $0.137$ ;  $MgO$ ,  $0.041$ ;  $CaO$ ,  $0.022$ ;  $ZnO$ ,  $0.132$ ;  $NiO$ ,  $0.119$ ; and  $V_2O_3$ ,  $0.078$ . Typical values are much lower. These elements may not be all contained in the Fe oxide host, but may be due to trace amounts of other minerals at the submicron level. Electron backscatter images show a density contrast at a very fine scale, which corre-

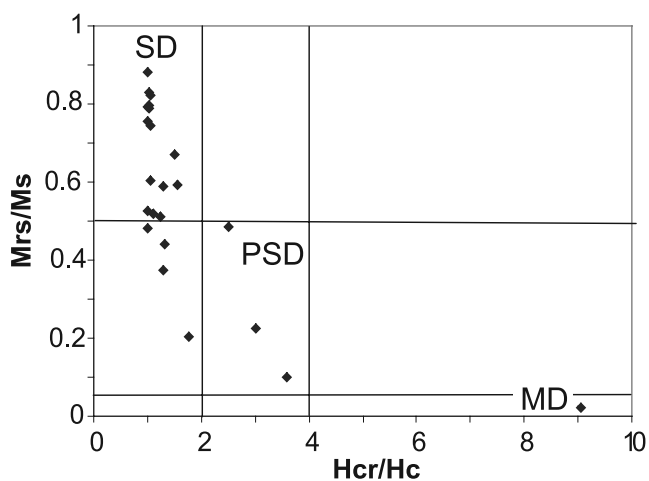


**Figure 9.** Plot of hysteresis properties of massive hematite-magnetite samples with  $M_{rs}/M_s$  values as high as  $0.80$  to  $0.90$  and  $H_{cr}/H_c$  ratios close to 1. The fields for SD, PSD, and MD grains [Dunlop and Özdemir, 1997] shown for visual guides are applicable to magnetite and cannot be necessarily applied to other minerals.

**Table 3.** Representative EMP Analyses, Cation Formulae, and Calculated End-Members of Magnetite, Sample 111-7b, Peculiar Knob

	Analysis				
	153	157	158	167	T117b
<i>Weight Percent Oxide</i>					
SiO <sub>2</sub>	0	0	0.013	0	0.001
TiO <sub>2</sub>	0.035	0.096	0.058	0.005	0.002
Al <sub>2</sub> O <sub>3</sub>	0	0.016	0.034	0.004	0.002
Cr <sub>2</sub> O <sub>3</sub>	0	0.006	0.009	0	0
V <sub>2</sub> O <sub>3</sub>	0	0	0.066	0	0
Fe <sub>2</sub> O <sub>3</sub>	68.945	68.260	68.492	69.123	68.418
MgO	0	0	0	0.002	0.009
NiO	0.026	0	0	0.004	0.001
Fe total	93.019	92.319	92.632	93.295	92.328
FeO	30.982	30.897	31.002	31.097	30.765
MnO	0.007	0	0	0.006	0.001
ZnO	0.077	0	0.009	0	0
CaO	0	0	0	0	0.005
Total	93.164	92.437	92.821	93.316	92.349
Total with Fe <sub>2</sub> O <sub>3</sub>	100.072	99.276	99.683	100.242	99.204
<i>Cations/3</i>					
Si	0.0000	0.0000	0.0005	0.0000	0.0000
Ti	0.0010	0.0028	0.0017	0.0001	0.0001
Al	0.0000	0.0007	0.0016	0.0002	0.0001
Cr	0.0000	0.0002	0.0003	0.0000	0.0000
V	0.0000	0.0000	0.0020	0.0000	0.0000
Fe <sup>3+</sup>	1.9980	1.9935	1.9918	1.9995	1.9997
Mg	0.0000	0.0000	0.0000	0.0001	0.0005
Ni	0.0008	0.0000	0.0000	0.0001	0.0000
Fe total	2.9958	2.9963	2.9937	2.9992	2.9990
Fe <sup>2+</sup>	0.9978	1.0028	1.0019	0.9997	0.9993
Mn	0.0002	0.0000	0.0000	0.0002	0.0000
Zn	0.0022	0.0000	0.0003	0.0000	0.0000
Ca	0.0000	0.0000	0.0000	0.0000	0.0002
Total cations Fe total	3.0000	3.0000	3.0000	3.0000	3.0000
Total Fe <sup>3+</sup> Fe <sup>2+</sup>	3.0000	3.0000	3.0000	3.0000	3.0000
Ox sum/3 cations	3.0010	3.0033	3.0041	3.0002	3.0001
4-Ox sum	0.9990	0.9967	0.9959	0.9998	0.9999
Fe <sup>3+</sup>	1.9980	1.9935	1.9918	1.9995	1.9997
Fe <sup>3+</sup> /Fe total	0.6669	0.6653	0.6653	0.6667	0.6668
<i>End-Members</i>					
Fe <sub>2</sub> SiO <sub>4</sub>	0	0	0.0502	0	0.0039
Fe <sub>2</sub> TiO <sub>4</sub>	0.1014	0.2802	0.1686	0.0145	0.0058
FeCr <sub>2</sub> O <sub>4</sub>	0	0.0092	0.0137	0	0
FeV <sub>2</sub> O <sub>4</sub>	0	0	0.1022	0	0
FeAl <sub>2</sub> O <sub>4</sub>	0	0.0366	0.0774	0.0091	0.0046
Sum	0.1014	0.3260	0.4122	0.0235	0.0143
MgFe <sub>2</sub> O <sub>4</sub>	0	0	0	0.0115	0.0521
FeFe <sub>2</sub> O <sub>4</sub>	99.5763	99.6740	99.5621	99.9331	99.9064
NiFe <sub>2</sub> O <sub>4</sub>	0.0805	0	0	0.0124	0.0031
MnFe <sub>2</sub> O <sub>4</sub>	0.0228	0	0	0.0195	0.0033
ZnFe <sub>2</sub> O <sub>4</sub>	0.2190	0	0.0257	0	0
CaFe <sub>2</sub> O <sub>4</sub>	0	0	0	0	0.0208
Sum	99.8986	99.6740	99.5878	99.9765	99.9857
Total	100.0000	100.0000	100.0000	100.0000	100.0000

sponds to a slight difference in optical reflectivity. Ideally pure hematite and also pure maghemite would contain 89.98 wt % FeO, whereas pure magnetite would contain 93.08 wt % FeO. Other than observing the weight percent total, there is no trick of formulation that will distinguish analyses of hematite from magnetite, and maghemite will have the same total as hematite. Any possible analytical distinction depends on the quality and reliability of the analyses, which we think are very high.

[41] For the 39 analyses of 246.6b (Figure 10a), the median value of the analytical sums is 89.70, where sums

below 89.20 were considered unacceptable. Aside from the peak centered approximately about the median, there are 6 analyses in the range 90.4–90.8 wt %. These 6 are concentrated in one part of the polished section, but few of them are contiguous. They can be interpreted as overlap analyses in regions of hematite containing approximately 17% of submicron magnetite or they can be interpreted as larger areas of magnetite-maghemite solid solution. Averaging over all 39 analyses would indicate a magnetite content of ~2.6% either as submicron patches or magnetite in solid solution with maghemite.

[42] For the 42 analyses of sample 242.2a (Figure 10b), the analytical sums are centered on three peaks at 90.10, 90.50, and 91.10. The two peaks with higher sums can be interpreted as overlap analyses in regions containing submicron magnetite or magnetite-maghemite. Further, there is nothing in the minor element analyses that is correlated with wt % FeO that would help distinguish hematite from magnetite, or could help distinguish maghemite replacing magnetite compared to hematite only. The hematite is quite pure with very little substitution of other elements.

[43] For the 46 analyses of sample 111.7b (Figure 10c), the analytical sums are centered on two peaks at 89.90 with 30 analyses between 88.90 and 90.70, and at 92.80 with 10 analyses between 92.30 and 93.50. In addition there are six analyses in an intermediate range 90.90 to 92.00. The 30 analyses near the first peak formulate excellently as near end-member hematite with corrected analytical sums 98.88 to 100.78 and calculated 99.68 to 99.99% of the Fe<sub>2</sub>O<sub>3</sub> end-member, where the calculation technique minimizes the end-member amount. The 10 analyses near the second peak formulate excellently as near end-member magnetite with corrected analytical sums 99.20 to 100.24 and calculated 99.56 to 99.93% of the FeFe<sub>2</sub>O<sub>4</sub> end-member, where the calculation technique minimizes that end-member amount. These analyses come from areas with generally lower optical reflectivity consistent with the presence of near-end-member magnetite. The six intermediate analyses give high totals formulated as hematite and low totals when formulated as magnetite, and, analytically, are best interpreted either as areas of hematite-magnetite overlaps, fine-grained intergrowths of hematite and magnetite, or as magnetite-maghemite solid solution.

## 4.2. Correlation of Mineral Chemistry and Rock Magnetic Properties

[44] The EMP data on the massive hematite-magnetite samples indicate that there is more than one Fe-oxide phase present in the large hematite grains. Numerous rock magnetic measurements show hematite and magnetite. The amount of magnetite is small; a conclusion based on the *J<sub>s</sub>*-T and *k*-T curves and hysteresis properties. This is also supported by the low bulk susceptibility of the massive ore samples. If one were to assume the bulk susceptibility is due to magnetite only, this would indicate 0.2–1% magnetite. Both high- and low-temperature data suggest a hematite with either magnetite or maghemite. Because maghemite has no known low-temperature transition, it is difficult to conclude definitively that maghemite is present, other than cases where samples show an irreversible decrease in magnetization above 300°C such as sample 247 (Figure 7a). Preliminary transmission electron microscopy shows the

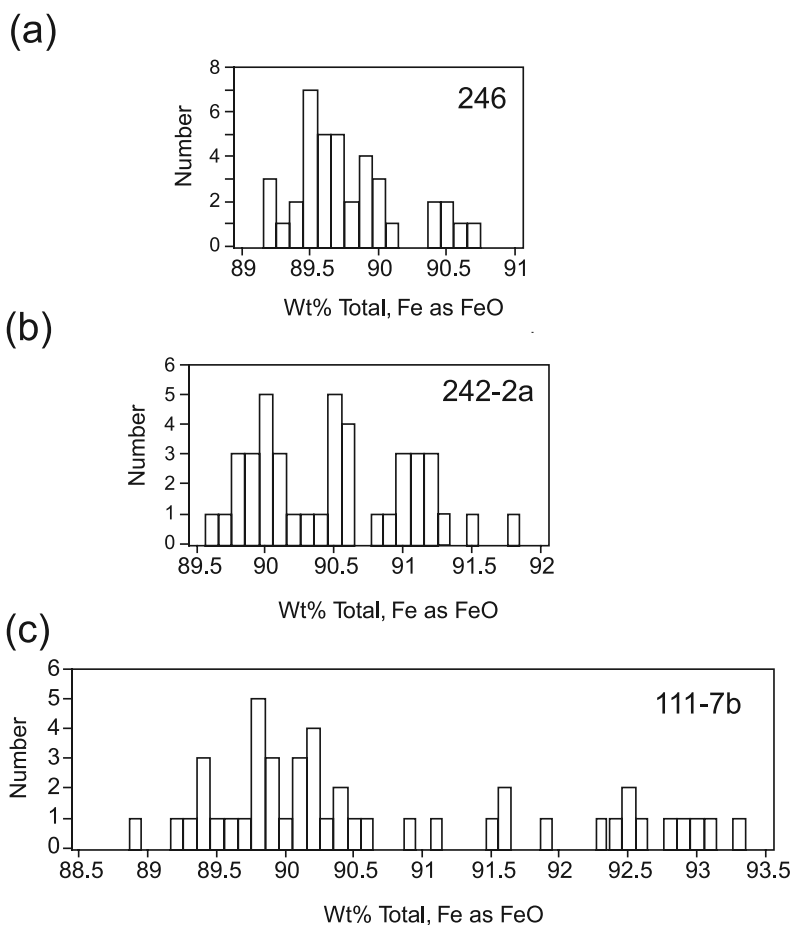


**Figure 10.** Histograms of the EMP analyses show the abundance of analyses reflecting a mixed oxide phase.

presence of a very fine intergrowth of either magnetite or maghemite [Schmidt *et al.*, 2005] but further work is needed to determine which of these two phases is intergrown in the hematite. The lattice parameters are very similar and the scale of the magnetite or maghemite is very small. Low-temperature data show that magnetic memory is retained to temperatures below the Verwey transition and the large recovery of hematite magnetization upon warming to room temperature is a feature we attribute to a magnetite or maghemite intergrowth in the hematite grains. Though these hematite grains are very large, some millimeter size, and have no visible exsolution, the bulk measured coercivities, up to 38 mT show that these grains behave like much finer grains. A fine-scale intergrowth of two phases suits the rock magnetic data and EMP data better than it suits coarse single-phase multidomain hematite.

## 5. Potential Field Modeling and the Poisson Theorem

[45] The gross geological structure in the cross section at 10500 mN on Figure 2 may be inferred from the drill hole logs (Figure 11). This allows the observed magnetic and gravity anomalies to be modeled. The magnetic signatures of the intersected bodies at Peculiar Knob have been modeled using a thick dike model (see algorithms of

Emerson *et al.* [1985]). Initially, vertically upward directed magnetization with an intensity of  $200 \text{ A m}^{-1}$  was tried. This yielded a magnetic anomaly of 50,000 nT, which is 60% higher than that observed, confirming the suggestion that the mean measured remanent intensity for the mHt/Mt bodies is higher than the true value. However, this result shows that remanent magnetization alone is sufficient to account for the observed magnetic anomaly.

[46] Since the main body that is intersected by DDH 85EN19 and DDH 85EN20 appears to be responsible for the major anomaly, further modeling was performed with a progressively weaker remanence for this body until the calculated anomaly agreed better with the observed anomaly. The remanent intensity value thus determined was  $120 \text{ A m}^{-1}$ , slightly less than the lower extreme of the estimate ( $190 \pm 70 \text{ A m}^{-1}$ ). A susceptibility of 0.25 SI was chosen as it is close to the average value for the six mHt/Ht sites and is considered to be close to the average value for the entire iron formation (Table 1). However, because the induced magnetization is less than 10% of the remanent magnetization this value is unimportant for the modeling.

[47] A finer refinement of the model involved adjusting the dip of the flanking body intersected by DDH 85EN21, while constraining the body to pass through the drill hole intersection point. Assigning dips to the three main bodies of  $60^\circ$ ,  $90^\circ$ , and  $95^\circ$  from northwest to southeast, respec-

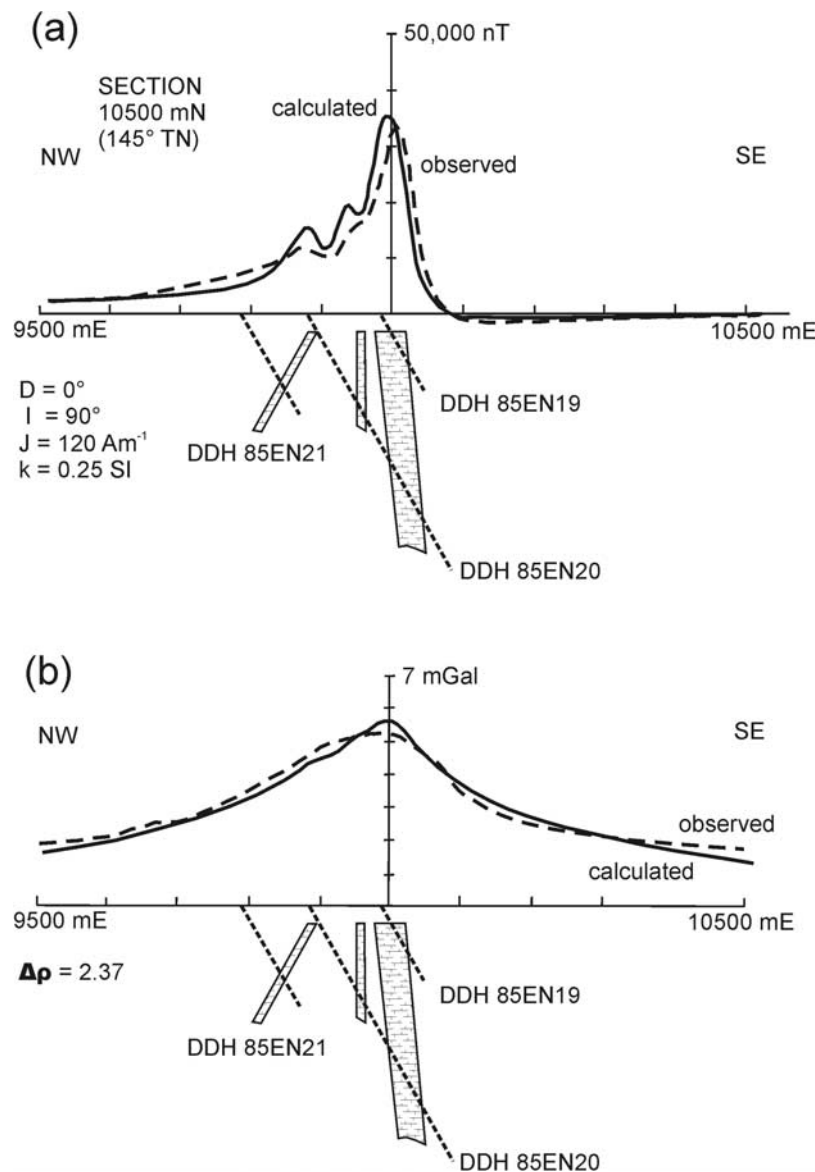


**Figure 11.** Two-dimensional models comparing the observed and calculated anomalies for Peculiar Knob for (a) magnetic and (b) gravity.

tively, was found to optimize the anomaly location. The fit of the calculated magnetic anomaly to the observed magnetic anomaly (Figure 11a) is reasonable, and although a somewhat better fit could be achieved by arbitrarily adjusting various parameters, it is preferable to keep the model as simple as possible for the model to represent the geology meaningfully. The same magnetic properties have been assigned to all bodies.

[48] As a further check on this model it was also used to calculate the gravity anomaly to compare with the observed Bouguer gravity anomaly. Estimates of densities of representative samples of the massive Ht/Mt and the host rocks led to use of a density contrast of  $2370 \text{ kg m}^{-3}$ . The resulting gravity anomaly is compared with the Bouguer anomaly in Figure 11b. Again there is a reasonable agreement between the calculated and the observed anomalies.

[49] The consistency of both the calculated magnetic and gravity anomalies and their observed counterparts can be

appreciated more by considering the Poisson Theorem [Blakely, 1996]. If a magnetic and a gravity anomaly arise from one source, as they appear to here, then even without assuming a source geometry, the magnetization and density contrasts can be related [Cordell and Taylor, 1971]. In the present instance this means that the gravitational source requires an intense vertical-up magnetization to match the observed magnetic anomaly, independently supporting the laboratory measurements.

## 6. Comparison of Magnetic Properties of Peculiar Knob With Those of Other Iron Formations

[50] The most comprehensive studies of magnetic properties of sedimentary Banded Iron Formations (BIF) are those undertaken on the Hamersley BIFs of Western Australia [Clark and Schmidt, 1986a, 1986b; Schmidt and Clark, 1994; Schmidt, 1998]. The Hamersley Basin covers

**Table 4.** Summary of Magnetic Properties of Australian Iron Formations<sup>a</sup>

Formation	$J$ , A m <sup>-1</sup>	$k$ , SI	Q	$k_{  }$ , SI	$k_{\perp}$ , SI	A
Boolgeeda <sup>b</sup>	~2.4	0.063 – 0.42	~0.1	-	-	-
Weeli Wolli	54.9	0.50	2.56	0.58	0.37	1.57
Joffre	16.0	0.27	1.37	0.35	0.14	2.50
Dales Gorge	27.8	0.59	1.10	0.72	0.35	2.06
Marra Mamba	25.6	0.71	0.85	0.79	0.58	1.36
Frere	<0.03	10 <sup>-3</sup>	<0.75	1.01 × 10 <sup>-3</sup>	0.98 × 10 <sup>-3</sup>	1.05
Peculiar Knob	120	0.25	12	0.26	0.23	1.10

<sup>a</sup> $J$ , intensity of magnetization;  $k$ , low-field magnetic susceptibility; Q, Koenigsberger ratio; A, anisotropy of magnetic susceptibility ( $k_{\max}/k_{\min}$ ). The Boolgeeda IF is from *Clark and Schmidt* [1994]; the Weeli Wolli IF, Joffre IF, Dales Gorge IF, and Marra Mamba IF are from *Schmidt* [1998]; and the Frere IF is from *Williams et al.* [2004].

<sup>b</sup>Samples of Boolgeeda IF are variable weathered. Both susceptibility and remanence are deleteriously affected although the former more so than the latter resulting in very low Koenigsberger ratios.

an area in excess of 300 km by 200 km. The Hamersley Group is about 2.5 km thick and contains several large units of BIF formed mostly by chemical sedimentation. In stratigraphic order these are the Marra Mamba Iron Formation (IF), the Dales Gorge (DG) and Joffre (J) Members of the Brockman IF, the Weeli Wolli IF, and the Boolgeeda IF.

[51] Mean magnetic properties for Australian IFs that have been studied are given in Table 4. The Koenigsberger ratios use a magnetic induction at the location of 53,600 nT. Note also that the effective Koenigsberger ratios depend on the bedding strike and dip, with respect to the inducing field, because the BIFs are also highly anisotropic. Typically the ratio of the parallel magnetic susceptibility to the perpendicular susceptibility (A) is about 2 (see *Clark and Schmidt* [1994] for full discussion).

[52] Samples of Boolgeeda IF are variably weathered and both susceptibility and remanence for this formation are deleteriously affected although the former more so than the latter resulting in an anomalously low Koenigsberger ratio. For the other Hamersley BIF remanences are typically 30 A m<sup>-1</sup> and bulk susceptibilities are about 0.6 SI. The NRMs of the Hamersley BIFs are carried by magnetite and are probably (thermo)chemical remanent magnetizations acquired during burial metamorphism of the precursor sedimentary iron formations [*Clark and Schmidt*, 1994].

[53] The Hamersley BIF shows a broad distribution of NRM and susceptibility values because of the nature of sampling banded strata where some specimens will inevitably contain more or less magnetic material depending on how many bands have been intersected. Nevertheless, average BIF properties greatly differ from those of the Peculiar Knob IF.

[54] It is worth making a cautionary note here regarding the uncritical use of large databases, such as that of *Schmidt* [1998] on the magnetic properties of the Hamersley BIFs. A favored method of geologists logging drill core is to use a pencil magnet to differentiate magnetite bands from hematite bands. This can dramatically affect the magnetic remanence of any low-coercivity magnetite bands within a few cm of the test zone. Low-temperature demagnetization can reduce spurious magnetizations of this nature but it is often not possible to reconstruct the NRM with confidence. Sharp changes of Koenigsberger ratios between contiguous specimens have also proven to be diagnostic. How remanence directions change on AF demagnetization is also useful. Sometimes it is necessary to make a value judgment based on all these factors. Other factors that must be taken into

account is the degree of alteration, either secondary mineralization or weathering. It is advisable to discard any drill core that contains mineralization or shows effects of weathering. The final arbiter on what are the appropriate properties of BIFs is magnetic modeling [*Clark and Schmidt*, 1994].

[55] An analysis of the database [*Schmidt*, 1998], after eliminating spurious data from mineralized and weathered samples, shows that more than 30% of the samples are weakly magnetic, with NRM values <2 A m<sup>-1</sup>, while fully 50% have NRMs less than 10 A m<sup>-1</sup>. NRM values for the entire Peculiar Knob IF are significantly higher than those of all the Hamersley BIFs. Almost 70% of the BIF samples have magnetizations ≤36 A m<sup>-1</sup>, the lowest measured NRM values for the mHt/Mt samples at Peculiar Knob, and only the granite and quartzite samples have NRMs ≤1 A m<sup>-1</sup>. Also in stark contrast with the Hamersley BIFs, the lowest susceptibility Peculiar Knob samples ( $k < 0.004$  SI) are rocks with an average NRM of 205 A m<sup>-1</sup>, whereas in the Hamersley BIF collection there is a very strong positive correlation between susceptibility and NRM. *Clark and Schmidt* [1994] attributed the relatively high Q values for MD magnetite-bearing rocks to the interaction between the magnetite grains in the magnetite bands of the BIFs.

[56] The Frere IF in the Earahedy Basin, Western Australia, is about 300–400 km SE of the Hamersley Ranges. Because this formation was sampled for paleomagnetic purposes [*Williams et al.*, 2004] only the facies low in iron and well away from the metamorphosed zones to the NW were sampled. The Frere IF is more strongly magnetic to the NW but exposures are weathered and have not been sampled. The results reported by *Williams et al.* [2004] were from deep (>100 m) commercially drilled core necessary to avoid the weathering that typically reached >50 m depth.

[57] The magnetic properties of some North American IFs are summarized in Table 5. Some of these properties have been obtained from oriented samples, while others are inferred from magnetic modeling. To some extent at least, the latter are the more reliable because many samples appear affected by lightning. This is particularly so for the North American studies which yielded very scattered remanence directions [*Alva-Valdivia and Urrutia-Fucugauchi*, 1995, 1998]. For the El Encino IF measured susceptibility and remanence values are given as 1 SI and 1 A m<sup>-1</sup>, whereas for two models the corresponding values required to match the magnetic survey data were found to be 0.01 SI and 35 A m<sup>-1</sup> and 0.0035 SI and 14 A m<sup>-1</sup>. The reason for

**Table 5.** Summary of Magnetic Properties of North American Iron Formations<sup>a</sup>

Formation	$J$ , A m <sup>-1</sup>	$k$ , SI	Q	$k_{  }$ (SI)	$k_{\perp}$ , SI	A
Biwabik						
Mesabi Main	-	1.10	low	1.40	0.70	2.00
Mesabi East	100	0.20	high	-	-	-
Algoman	11.0	1.17	0.20 <sup>b</sup>	1.36	0.78	1.75
Sherman	25.0	1.69	0.31	1.93	1.21	1.60
Archean	12.1	0.80	0.32	0.92	0.57	1.61
Gunflint <sup>c</sup>	0.45	0.015	0.76	0.013	0.012	1.08
El Encino	14–35 <sup>d</sup>	0.0035–0.01	30–102	-	-	-
Las Truchos	>300 <sup>e</sup>	0.30	20?	-	-	-
Sokoman	3.7	0.207	0.48	0.214	0.193	1.10

<sup>a</sup> $J$ , intensity of magnetization;  $k$ , low-field magnetic susceptibility; Q, Koenigsberger ratio; A, anisotropy of magnetic susceptibility ( $k_{\max}/k_{\min}$ ). Biwabik is from *Bath* [1962]; Algoman is from *Symons et al.* [1980]; Sherman is from *Symons and Stupavsky* [1979]; Archean is from *Symons et al.* [1981]; Gunflint is from *Schmidt and Williams* [2003]; El Encino is from *Alva-Valdivia and Urrutia-Fucugauchi* [1995]; Las Truchos is from *Alva-Valdivia and Urrutia-Fucugauchi* [1998]; and Sokoman is from *Williams and Schmidt* [2004].

<sup>b</sup>Q values have been recalculated as described in the text.

<sup>c</sup>Only values for the more magnetic upper taconite are given here. Also the bulk value is greater than the mean bedding parallel value for the susceptibility because the bulk value is a simple arithmetic mean whereas the bedding parallel and perpendicular values are from oriented tensor means, which behave similarly to the resultant (R) of N unit vector means ( $R < N$ ).

<sup>d</sup>Measured susceptibility and remanence are given as 1 SI and 1 A m<sup>-1</sup>, but directions are scattered. The values are from model values that are required to match magnetic survey data.

<sup>e</sup>These are extremely high values. The fact that the samples are from exposed outcrops and their directions are scattered suggests the high values are related to lightning strikes.

these discrepancies is unknown but values in Table 5 are the model values.

[58] The Biwabik IF from the East Mesabi district also requires a strong remanence to model magnetic survey data [*Bath*, 1962]. Contact metamorphism of the Biwabik IF caused by the intrusion of the Duluth gabbro near East Mesabi has produced a remanence of 100 A m<sup>-1</sup> directed within the bedding plane. Elsewhere, the Biwabik IF is not extremely magnetic, e.g., Mesabi Main district, and the magnetization is dominated by the induced components.

[59] Other bodies with significant remanent magnetization are the Algoman IF [*Symons et al.*, 1980] with a value of 11 A m<sup>-1</sup>, the Sherman IF [*Symons and Stupavsky*, 1979] with a value of 25 A m<sup>-1</sup>, and an Archean IF [*Symons et al.*, 1981] with a value of 12 A m<sup>-1</sup>. These formations are all from Ontario. The Koenigsberger ratios given in Table 4 for these three bodies have been recalculated since the values quoted (Q = 0.63, 0.46 and 0.67, respectively) seem to be too high. For instance, assuming  $H = 48$  A m<sup>-1</sup> ( $B = 60$   $\mu$ T as given),  $Q = J/kH = 11/(1.17 \times 48) = 0.20$  for the Algoman IF. Similarly, for the Sherman IF a value of 0.46 is given by *Symons and Stupavsky* [1979], but Q = 0.31 is calculated here and for the Archean IF where *Symons et al.* [1981] record a value of 0.67 and Q = 0.32 is calculated here, again assuming  $H = 48$  A m<sup>-1</sup>. Nevertheless, the remanences of these bodies fall an order of magnitude short of the remanence from the Peculiar Knob IF. The magnetization of most of the iron formations included in Tables 4 and 5 are dominated by magnetite, whereas hematite is the dominant remanence carrier at Peculiar Knob.

[60] The magnetization of the Peculiar Knob IF is overwhelmingly dominated by remanence, which is interpreted as a stable, ancient ( $\sim 1590$  Ma) TRM acquired during high-grade metamorphism. Koenigsberger ratios are extremely high, in some cases being much greater than 100. Remanent intensities range from 36 to 227 A m<sup>-1</sup> with a measured average  $\sim 190$  A m<sup>-1</sup>, although modeling shows that the true value is closer to 120 A m<sup>-1</sup> (Table 1).

[61] The magnetic anomalies over the Hamersley Basin can be up to 15,000 nT; however, a significant component of the magnetization is induced by the Earth's field. The anomaly over the Peculiar Knob deposit is 30,000 nT and is dominated by remanence. The Peculiar Knob IF would have a large magnetic anomaly associated with it in the absence of an inducing field such as the local Earth's field, and from this perspective the mineralogy found at Peculiar Knob should be studied in detail to help us understand the types of minerals and fine-scale intergrowths needed to produce such large remanent magnetizations on Earth and on planets such as Mars that no longer have a magnetic field.

## 7. Summary

[62] The Peculiar Knob Fe deposit is buried under 30 m of sediment. This metamorphosed hematite ore carries a very high magnetization that is accurately modeled using potential field methods. A simple geological model explains both the observed magnetic and gravity anomalies consistent with the Poisson theorem. The magnetization of the metamorphosed iron formation is overwhelmingly dominated by remanence, with intensities ranging from 36 to 227 A m<sup>-1</sup> with an average  $\sim 190$  A m<sup>-1</sup>, although magnetic modeling is more consistent with a true mean of 120 A m<sup>-1</sup>. This reflects bias in sampling whereby rock types that were more magnetic were sampled. Koenigsberger ratios are extremely high, in some cases  $>100$ .

[63] We postulate that acquisition of TRM by coarse-grained hematite, probably augmented and stabilized by fine intergrowths of magnetite/maghemite with hematite accounts for the strong remanent magnetization. The massive hematite samples measured here show significantly higher bulk coercivities (up to 38 mT) than can be attributed to monophasic multidomain hematite with low coercivities in the range of 3 to 13 mT [*Halgedahl*, 1998; *Kletetschka et al.*, 2000a]. Fine intergrowths of maghemite, or magnetite in a hematite host would generate a high magnetization and provide a mechanism to generate higher coercivity, which aids in the retention of the magnetic memory.

[64] The Peculiar Knob IF was metamorphosed over 1 billion years ago. The present-day magnetic signature is dominated by the remanence acquired when this material cooled in the Mesoproterozoic. Coarse-grained hematite with ultrafine intergrowths similar to that encountered in this study, if cooled from high temperatures, can carry strong and stable TRM that could account for the magnitude of anomalies found on Mars.

[65] **Acknowledgments.** We thank CRA Exploration (now Rio Tinto) for initiating this work in 1986 and providing technical and potential field information. Mark Huddleston assisted during fieldwork and sample preparation. We thank Nathan Daczko and Norman Pearson at Macquarie University, New South Wales, for microprobe assistance and analyses; the Institute for Rock Magnetism, University of Minnesota, for a visiting

fellowship to S.M. supported by NSF; and BGI under the EU 'IHP-Access to research Infrastructures Program (contract HPRI-1999-CT-00004). S.M. was supported by the Norwegian National Research Council (grants 163556/S10 and 169470/S30).

## References

- Acuña, M. H., et al. (1999), Global distribution of crustal magnetization discovered by the Mars Global Surveyor MAG/ER experiment, *Science*, *284*, 790–793.
- Alva-Valdivia, L. M., and J. Urrutia-Fucugauchi (1995), Rock magnetism and magnetic surveys in the iron ore deposit of El Encino, Mexico, *J. S. Am. Earth Sci.*, *8*, 209–220.
- Alva-Valdivia, L. M., and J. Urrutia-Fucugauchi (1998), Rock magnetic properties and ore microscopy of the iron ore deposit of Las Truchas, Michoacan, Mexico, *J. Appl. Geophys.*, *38*, 227–299.
- Balsley, J. R., and A. F. Buddington (1958), Iron titanium oxide minerals, rocks, and aeromagnetic anomalies of the Adirondack area, New York, *Econ. Geol.*, *53*, 777–805.
- Bath, G. D. (1962), Magnetic anomalies and magnetizations of the Biwabik iron-formation, Mesabi area, Minnesota, *Geophysics*, *27*, 627–650.
- Blakely, R. J. (1996), *Potential Theory in Gravity and Magnetic Applications*, 441 pp., Cambridge Univ. Press, New York.
- Brown, L. B., S. A. McEnroe, and R. J. Harrison (2005), Rock-magnetic properties of samples from the El Laco magnetite “flow”, High Andes, Chile, *Eos Trans. AGU*, *86*(52), Fall Meet. Suppl., Abstract GP41A-0856.
- Clark, D. A. (1997), Magnetic petrophysics and magnetic petrology: Aids to geological interpretation of magnetic surveys, *AGSO J. Aust. Geol. Geophys.*, *17*, 83–103.
- Clark, D. A. (1999), Magnetic petrology of igneous intrusions: Implications for exploration and magnetic interpretation, *Explor. Geophys.*, *30*, 5–26.
- Clark, D. A., and P. W. Schmidt (1986a), Magnetic properties of the banded-iron formations of the Hamersley Group, W. A., *Rep. RIR 1638R*, 33 pp. and appendices, CSIRO Div. of Miner. Phys. and Mineral., North Ryde, N. S. W., Australia.
- Clark, D. A., and P. W. Schmidt (1986b), Geological structure and magnetic signatures of the Hamersley BIFS, *Rep. RIR 1639R*, 17 pp. and appendices, CSIRO Div. of Miner. Phys. and Mineral., North Ryde, N. S. W., Australia.
- Clark, D. A., and P. W. Schmidt (1994), Magnetic properties and magnetic signatures of BIFs of the Hamersley Basin and Yilgarn Block, Western Australia, in *Geophysical Signatures of Western Australian Mineral Deposits*, edited by M. C. Dentith et al., *Publ. 26*, pp. 343–354, Geol. and Geophys. Dep., Univ. of West. Aust., Perth.
- Connerney, J. E. P., M. H. Acuna, N. F. Ness, T. Spohn, and G. Schubert (2004), Mars crustal magnetism, *Space Sci. Rev.*, *111*, 1–32.
- Cordell, L., and P. T. Taylor (1971), Investigations of magnetization and density of a North American seamount using Poisson's theorem, *Geophysics*, *36*, 919–937.
- Dunlop, D. J., and Ö. Özdemir (1997), *Rock Magnetism: Fundamentals and Frontiers*, 573 pp., Cambridge Univ. Press, New York.
- Emerson, D. W., D. A. Clark, and S. J. Saul (1985), Magnetic exploration models incorporating remanence, demagnetisation and anisotropy: HP 41C handheld computer algorithms, *Explor. Geophys.*, *16*, 1–122.
- Esdale, D., D. Pridmore, J. Coggon, P. Muir, P. Williams, and F. Fritz (2003), Olympic dam copper-uranium-gold-silver-rare earth element deposit, South Australia: A geophysical case history, in *Geophysical Signatures of South Australian Mineral Deposit*, edited by M. C. Dentith, *Publ. 31*, pp. 147–168, Cent. for Global Metal., Univ. of West. Aust., Perth.
- Frandsen, C., S. L. S. Stipp, S. A. McEnroe, M. B. Madsen, and J. M. Knudsen (2004), Magnetic force microscopy (MFM) reveals magnetic domain structure and stray field of individual elongated magnetite grains, *Phys. Earth Planet. Inter.*, *141*, 121–124.
- Halgedahl, S. L. (1998), Barkhausen jumps in large versus small platelets of natural hematite, *J. Geophys. Res.*, *103*, 30,575–30,589.
- Hargraves, R. B. (1959), Magnetic anisotropy and remanent magnetism in hemo-ilmenite from ore deposits at Allard Lake, Quebec, *J. Geophys. Res.*, *64*, 1565–1578.
- Hargraves, R. B., J. M. Knudson, M. B. Madsen, and P. Bertelsen (2001), Finding the right rocks on Mars, *Eos Trans. AGU*, *82*, 292.
- Hart, J., and H. Freeman (2003), Geophysics of the Prominent Hill prospect, South Australia, in *Geophysical Signatures of South Australian Mineral Deposits*, edited by M. C. Dentith, *Publ. 31*, pp. 93–100, Cent. for Global Metal., Univ. of West. Aust., Perth.
- Hrouda, F., A. Stephenson, and L. Wolter (1983), On the standardization of measurements of magnetic susceptibility, *Phys. Earth Planet. Inter.*, *32*, 203–208.
- Kelso, P. P., S. K. Banerjee, and C. Teyssier (1993), Rock magnetic properties of the Arunta Block, central Australia and their implications for the interpretation of long-wavelength anomalies, *J. Geophys. Res.*, *98*, 15,987–15,999.
- Kletetschka, G., P. J. Wasilewski, and P. T. Taylor (2000a), Hematite vs. magnetite as the signature for planetary magnetic anomalies?, *Phys. Earth Planet. Inter.*, *119*, 259–267.
- Kletetschka, G., P. J. Wasilewski, and P. T. Taylor (2000b), Unique thermoremanent magnetization of multidomain sized hematite: Implications for magnetic anomalies, *Earth Planet. Sci. Lett.*, *176*, 469–479.
- McEnroe, S. A., and L. L. Brown (2000), A closer look at remanence dominated anomalies: Rock-magnetic properties and magnetic mineralogy of the Russell Belt microcline-sillimanite gneisses, northwestern Adirondacks mountains, New York, *J. Geophys. Res.*, *105*, 16,437–16,456.
- McEnroe, S. A., R. Harrison, P. Robinson, U. Golla, and M. J. Jercinovic (2001a), The effect of fine-scale microstructures in titanohematite on the acquisition and stability of NRM in granulite facies metamorphic rocks from southwest Sweden: Implications for crustal magnetism, *J. Geophys. Res.*, *106*, 30,523–30,546.
- McEnroe, S. A., P. Robinson, and P. T. Panish (2001b), Aeromagnetic anomalies, magnetic petrology and rock magnetism of hemo-ilmenite- and magnetite-rich cumulates from the Sokndal region, south Rogaland, Norway, *Am. Mineral.*, *86*, 1447–1468.
- McEnroe, S. A., R. Harrison, P. Robinson, and F. Langenhorst (2002), Nanoscale hematite-ilmenite lamellae in massive ilmenite rock: An example of lamellar magnetism with implications for planetary magnetic anomalies, *Geophys. J. Int.*, *151*, 890–912.
- McEnroe, S. A., L. L. Brown, and P. Robinson (2004a), Earth analog for Martian anomalies: Remanence properties of hemo-ilmenite nodules in the Bjerkreim-Sokndal intrusion, Rogaland, Norway *J. Appl. Geophys.*, *56*, 195–212.
- McEnroe, S. A., J. R. Skilbrei, P. Robinson, F. Heidelbach, F. Langenhorst, and L. L. Brown (2004b), Magnetic anomalies, layered intrusions and Mars, *Geophys. Res. Lett.*, *31*, L19601, doi:10.1029/2004GL020640.
- McEnroe, S. A., F. Langenhorst, P. Robinson, G. Bromiley, and C. Shaw (2004c), What's magnetic in the lower crust?, *Earth Planet. Sci. Lett.*, *226*, 175–192.
- McEnroe, S. A., R. J. Harrison, M. Jackson, A. M. Hirt, P. Robinson, F. Langenhorst, T. Kasama, A. Putnis, L. L. Brown, and U. Golla-Schindler (2005a), Lamellar magnetism: Effects of interface versus exchange interactions of nanoscale exsolutions in the ilmenite-hematite system, *J. Phys. Conf. Ser.*, *17*, 154–167.
- McEnroe, S. A., A. M. Hirt, P. Robinson, R. J. Harrison, and L. B. Brown (2005b), The effects of nanoscale exsolution on magnetic properties: Insights from Forc diagrams, *Eos Trans. AGU*, *86*(52), Fall Meet. Suppl., Abstract GP41A-0864.
- McFadden, P. L., and A. B. Reid (1982), Analysis of palaeomagnetic inclination data, *Geophys. J. R. Astron. Soc.*, *69*, 307–319.
- Morris, B. J., and J. K. Hough (1997), South Australia Steel and Energy Project, Peculiar Knob Prospect, South Australia, *Rep. Book 97/9*, Dep. of Mines and Energy Resour., Adelaide, Queensl., Australia.
- Özdemir, Ö., and D. J. Dunlop (2002), Thermoremanence and stable memory of single-domain hematites, *Geophys. Res. Lett.*, *29*(18), 1877, doi:10.1029/2002GL015597.
- Özdemir, Ö., and D. J. Dunlop (2005), Thermoremanent magnetization of multidomain hematite, *J. Geophys. Res.*, *110*, B09104, doi:10.1029/2005JB003820.
- Pinto, M. J., and M. O. McWilliams (1990), Drilling-induced isothermal remanent magnetization, *Geophysics*, *55*, 111–115.
- Ridley, B. H., and H. E. Brown (1980), The transformer bridge and magnetic susceptibility measurement, *Bull. Aust. Soc. Explor. Geophys.*, *11*, 110–114.
- Robinson, P., R. J. Harrison, S. A. McEnroe, and R. Hargraves (2002), Lamellar magnetism in the hematite-ilmenite series as an explanation for strong remanent magnetization, *Nature*, *418*, 517–520.
- Robinson, P., R. J. Harrison, S. A. McEnroe, and R. Hargraves (2004), Nature and origin of lamellar magnetism in the hematite-ilmenite series, *Am. Mineral.*, *89*, 725–747.
- Schmidt, P. W. (1986), Magnetic properties and models for Peculiar Knob and Teatree Glen prospects, S. A., *Rep. RIR 1659R*, 27 pp., CSIRO Div. of Miner. Phys. and Mineral., North Ryde, N. S. W., Australia.
- Schmidt, P. W. (1998), Magnetic petrophysical database for Hamersley Basin BIFs, WA, *Rep. 535C*, pp. 19 plus appendices and data disk, CSIRO Explor. and Min. North Ryde, N. S. W., Australia.
- Schmidt, P. W., and D. A. Clark (1994), Palaeomagnetism and magnetic anisotropy of Proterozoic banded-iron formations and iron ores of the Hamersley Basin, Western Australia, *Precambrian Res.*, *69*, 133–155.
- Schmidt, P. W., and G. E. Williams (2003), Reversal asymmetry in Mesoproterozoic overprinting of the 1.88-Ga Gunflint Formation, Ontario,

- Canada: Non-dipole effects or apparent polar wander?, *Tectonophysics*, 377, 7–32.
- Schmidt, P. W., S. A. McEnroe, P. Robinson, and D. Clark (2005), Inter-growths in multidomain hematite: Source of high NRM intensities and coercivity?, *Eos Trans. AGU*, 86(52), Fall Meet. Suppl., Abstract, GP41A-0865.
- Scott, E. R. D., and M. Fuller (2004), A possible source for the Martian crustal magnetic field, *Earth Planet. Sci. Lett.*, 220, 83–90.
- Symons, D. T. A., and M. Stupavsky (1979), Magnetic characteristics of the iron formation near Temagami, Ontario, *Ont. Geol. Surv. Misc. Pap.*, 87, 133–147.
- Symons, D. T. A., D. S. Walley, and M. Stupavsky (1980), Component magnetization of the Algoman iron formation and host rocks, Moose Mountain Mine, Ontario, *Ont. Geol. Surv. Misc. Pap.*, 93, 198–214.
- Symons, D. T. A., A. W. Quick, and M. Stupavsky (1981), Magnetic and paleomagnetic characteristics of the Archean iron formation and host rocks at the Adams Mine, Ontario, *Ont. Geol. Surv. Misc. Pap.*, 98, 293–307.
- Veitch, R. J., I. Hedley, and J.-J. Wagner (1983), Magnetic anisotropy calibration error, *Geophys. J. R. Astron. Soc.*, 75, 407–409.
- Williams, G. E., and P. W. Schmidt (2004), Paleomagnetism of the 1.88-Ga Sokoman Formation in the Schefferville-Knob Lake area, Québec, Canada, and implications for the genesis of iron oxide deposits in the central New Québec Orogen, *Precambrian Res.*, 128, 167–188.
- Williams, G. E., P. W. Schmidt, and D. A. Clark (2004), Paleomagnetism of iron-formation from the late Palaeoproterozoic Frere Formation, Earraheedy Basin, Western Australia: Palaeogeographic and tectonic implications, *Precambrian Res.*, 128, 367–383.

---

D. A. Clark and P. W. Schmidt, CSIRO Industrial Physics, PO Box 218, Lindfield, NSW 2070, Australia. (phil.schmidt@csiro.au)

S. A. McEnroe and P. Robinson, Geological Survey of Norway, N-7491 Trondheim, Norway.